Anti-HVEM mAb therapy improves antitumoral immunity both in vitro and in vivo, in a novel transgenic mouse model expressing human HVEM and BTLA molecules challenged with HVEM expressing tumors

Clémence Demerlé,[1,2] Laurent Gorvel [ID] ,[1,2] Marielle Mello,[3] Sonia Pastor,[2] Clara Degos,[1,2] Ana Zarubica,[3] Fabien Angelis,[3] Frédéric Fiore [ID] ,[3] Jacques A Nunes [ID] ,[2] Bernard Malissen,[3] Laurent Greillier,[4] Geoffrey Guittard [ID] ,[2] Hervé Luche,[3] Fabrice Barlesi,[5] Daniel Olive [ID] [1,2]

ABSTRACT

Background Tumor necrosis factor superfamily member 14 (TNFRSF14)/herpes virus entry mediator (HVEM) is the ligand for B and T lymphocyte attenuator (BTLA) and CD160-negative immune co-signaling molecules as well as viral proteins. Its expression is dysregulated with an overexpression in tumors and a connection with tumors of adverse prognosis.

Methods We developed C57BL/6 mouse models co-expressing human (hu)BTLA and huHVEM as well as antagonistic monoclonal antibodies (mAbs) that completely prevent the interactions of HVEM with its ligands.

Results Here, we show that the anti-HVEM18-10 mAb increases primary human αβ-T cells activity alone (CIS-activity) or in the presence of HVEM-expressing lung or colorectal cancer cells in vitro (TRANS-activity). Anti-HVEM18-10 synergizes with antiprogrammed death-ligand 1 (anti-PD-L1) mAb to activate T cells in the presence of PD-L1-positive tumors, but is sufficient to trigger T cell activation in the presence of PD-L1-negative cells. In order to better understand HVEM18-10 effects in vivo and especially disentangle its CIS and TRANS effects, we developed a knockin (KI) mouse model expressing human BTLA (huBTLA^{+/+}) and a KI mouse model expressing both huBTLA^{+/+}/huHVEM^{+/+} (double KI (DKI)). In vivo preclinical experiments performed in both mouse models showed that HVEM18-10 treatment was efficient to decrease human HVEM^{+} tumor growth. In the DKI model, anti-HVEM18-10 treatment induces a decrease of exhausted CD8^{+} T cells and regulatory T cells and an increase of effector memory CD4^{+} T cells within the tumor. Interestingly, mice which completely rejected tumors (±20%) did not develop tumors on rechallenge in both settings, therefore showing a marked T cell-memory phenotype effect.

Conclusions Altogether, our preclinical models validate anti-HVEM18-10 as a promising therapeutic antibody to use in clinics as a monotherapy or in combination with existing immunotherapies

WHAT IS ALREADY KNOWN ON THIS TOPIC

⇒ Immunotherapies (IT) and immune checkpoint inhibitors (ICI) opened a new era in cancer treatment leading to major clinical benefits in only subgroups of patients pushing the research toward the development of another ICI.

⇒ TNFRSF14/HVEM is the ligand for B and T lymphocyte attenuator (BTLA) and CD160-negative immune co-signaling molecules as well as viral proteins and is overexpressed in tumors concurring to tumors adverse prognosis.

WHAT THIS STUDY ADDS

⇒ To study the therapeutic effect of antagonist HVEM monoclonal antibodies in an immunocompetent and dynamic environment, we developed C57BL/6 mouse models co-expressing human (hu) BTLA and huHVEM.

⇒ Anti-HVEM allowed the in vitro co-activation of T cells and its injection in mice induced the development of a marked T cell-memory phenotype with the development of tumor antigen-specific T cells contributing in HVEM[+] tumor reduction or rejection.

HOW THIS STUDY MIGHT AFFECT RESEARCH, PRACTICE OR POLICY

⇒ Altogether, these results highlight the interest of anti-HVEM IT alone or in combination with another IT to further enhance antitumor immunity in clinic.

(antiprogrammed cell death protein 1/anti-PD-L1/anti-cytotoxic T-lymphocyte antigen-4 (CTLA-4)).

INTRODUCTION

Immunotherapies (IT) and immune checkpoint inhibitors (ICI) opened a new era in cancer treatment. ICI unleash antitumoral

immune responses, leading to major clinical benefits in subgroups of patients. However, rate and duration of IT successes are variable among cancer types and patients. Indeed, in lung cancer antiprogrammed cell death protein 1 (anti-PD-1)/programmed death-ligand 1 (PD-L1) antagonistic antibodies offer a durable remission in 30% of patients.[1 2] However, in colorectal cancer, the efficacy of anti-PD-1/PD-L1 was restricted to a small subset of patients presenting a high microsatellite instability status.[3 4] Consequently, new IT targets and approaches are needed to achieve efficacy in a larger proportion of patients.

HVEM, or TNFRSF14, is a TNF-receptor family member largely expressed by healthy immune and non-immune cells and participates to immune homeostasis.[5 6] HVEM is also upregulated in numerous solid and hematological malignancies such as melanoma,[7] digestive cancers,[8 9] or breast cancer.[10] HVEM network of interactors is complex and induces either cell activation or inhibition.[11] Indeed, HVEM binding to B and T lymphocyte attenuator (BTLA) and CD160 (BY55) triggers co-inhibitory signals whereas its binding to LIGHT (TNFSF14) and lymphotoxin-α are co-stimulatory . Similar to PD-1 and CTLA-4, BTLA is an important co-inhibitory receptor expressed by B and T cells.[12] Therefore, targeting HVEM is a promising but complex IT strategy.[13]

In our study, we focused on lung and colorectal cancer that are two of the most worldwide common cancers in both men and women. In colorectal cancer, HVEM upregulation in malignant lesions is linked to tumor status and pathological stage, with an independent prognostic value.[8] In lung cancer, HVEM expression seems to be a tumor driven mechanism, independent from the PD-L1 network that may contribute to immune escape.[14]

Our team previously described a monoclonal anti-HVEM monoclonal antibody (mAb) (anti-HVEM18-10) that preferentially inhibits HVEM interaction with BTLA and enhances γδ-T cells responses against lymphoma.[15] Here, we further evaluate the CIS-activity and TRANS-activity of anti-HVEM18-10. CIS-activity represents the antibody binding on effector HVEM$^+$CD4$^+$ and HVEM$^+$CD8$^+$ T cells directly in the absence of huHVEM$^+$ target cell lines. TRANS-activity is measured by checking immune cell activation in the presence of a HVEM$^+$ cell line in co-culture. We also show the interest of anti-HVEM18-10 combination with other ICIs such as anti-PD-L1 mAb, although HVEM18-10 alone is sufficient to trigger T cell activation in the absence of PD-L1 expression. In order to better understand HVEM18-10 mAb effect in vivo, we developed an innovative syngeneic immunocompetent mouse model expressing human BTLA (huBTLA$^{+/+}$) or both human BTLA and human HVEM (huBTLA$^{+/+}$huHVEM$^{+/+}$, (double KI (DKI)). Our experiments performed in both mouse models showed that anti-HVEM18-10 treatment was efficient to decrease tumor growth and strengthened local immune response. Moreover, the rechallenge of tumor-free mice (20% of treated mice) demonstrates that the immune response is durable with a marked memory T cells phenotype.

Altogether, our preclinical data validate anti-HVEM18-10 as a promising antibody to use in clinics alone or in combination with existing therapies (anti-PD-1/anti-PD-L1/anti-CTLA-4).

METHODS
Antibodies
Anti-HVEM18-10 and anti-PD-L1 3.1 are homemade antibodies that have been described previously.[15 16] Briefly, mAbs are murine IgG1 antihuman HVEM or PD-L1 mAb, produced as ascites and purified by protein A binding and elution with the Affi-gel Protein A MAPS II Kit (Bio-Rad, Marnes-La-Coquette, France). Mouse IgG1 isotype control was purchased from Miltenyi Biotec (Bergisch Gladbach, Germany).

Transcriptomic expression of HVEM and PD-L1
To study the transcriptomic expression of HVEM and PD-L1 data were extracted from The Cancer Genome Atlas (TCGA) database containing 526 lung adenocarcinoma samples and 388 colorectal carcinoma samples. Tumor cell lines gene expression values were extracted from the Cancer Cell Line Encyclopedia. Data were normalized and expressed as log2(TPM+1) of raw value.

Co-culture and proliferation assays
After thawing and overnight resting in RPMI supplemented with 10% fetal calf serum, peripheral blood mononuclear cells (PBMCs) were stained with Cell Trace Violet (Thermo isher) according to manufacturer's instructions. Co-culture assays were there performed during 72 hours and described in online supplemental material.

Knockin mouse model
Generation and genotyping of B6-Tnfrsf14^{tm1Ciphe} and Btla^{Tm1Ciphe} are described in online supplemental material. Mice were bred and maintained under specific pathogen-free conditions at the CIPHE animal facility.

Experimental tumor growth experiments
Single-cell suspensions of MC-38 or MC-38^{huHVEM} colorectal cancer cells were injected (0.5×10^6 for neo challenge, 2×10^6 for rechallenge) subcutaneously in the right flank of huBTLA$^{+/+}$huBTLA$^{+/+}$ mice. Mice bearing tumor between 50 and 100 mm^3 were then randomized at day 9 and mice were injected with an isotype control (2 mg/kg or 10 mg/kg) or anti-HVEM18-10 (2 mg/kg or 10 mg/kg) or CTLA-4 antibody (2 mg/kg) every 3–4 days with for a total of six injections.

Tumor preparation for mass cytometry and immunoprofiling
Tumors were resected from huBTLA$^{+/+}$ and DKI mice which received anti-HVEM18-10, anti-CTLA-4, or isotype treatment. Tumors were collected and digested using the Tumor Dissociation Kit (Miltenyi Biotech). Single cells

Table 1 Flow cytometry panel for HVEM expression on T cells subsets

Marker	Fluorochrome	Isotype
CD27	BV605	
CD45RA	BV711	
CD45	BV786	
CD8	PE	
7AAD	PeCy5	
CD56	PeCy7	
HVEM	APC	IgG1-APC
CD3	APCCy7	

suspension was then prepared and stained then acquired on a Helios mass cytometer (Cy-TOF, Fluidigm) and analyzed using the OMIQ software platform (OMIQ). Protocol is detailed in online supplemental method.

Unsupervised CyTOF data clustering and phenotypic analysis

CyTOF data files were exported (Helios program, Fluidigm), debarcoded and live cells were gated in FlowJo (Treestar, BD). Live cell.*fcs* files were exported and analyzed using OMIQ online platform (OMIQ).[17] Detailed protocol for data clustering and phenotypic analysis is described in online supplemental method. All used panels are shown in tables 1–4.

RESULTS

HVEM is highly expressed on T cells and the blockade of HVEM in CIS enhances T cell activation

We first studied the effect of anti-HVEM18-10 blockade directly on T cells (CIS-blockade). PBMCs were isolated from healthy donors and stimulated for 72 hours with anti-CD3 in combination with anti-HVEM18-10 or an IgG1 control mAbs. We found that HVEM was highly expressed on activated CD4$^+$ and CD8$^+$ T cells (figure 1A,B). HVEM expression is increased on stimulation in CD4$^+$ T cells (figure 1A), this effect was marked on CD4$^+$ effector memory T cells (figure 1C). HVEM expression did not differ on CD8$^+$ T cell, on stimulation or memory subtypes (figure 1B,D). HVEM is highly expressed on less

Table 2 Flow cytometry panel for proliferation assay

Marker	Fluorochrome
CD45	BV786
CD3	PeCF594
CD4	BV605
CD8	APC
CD56	PeCy7
Tgd	PE
7AAD	PeCy5
CD25	FITC
CTV	V450

Table 3 Panel for tumor infiltrating lymphocytes exploration with mass cytometry (Ext238)

Marker	Metal
CD11b	115In
CD4	141Pr
CD357	143Nd
CD45R	144Nd
CD69	145Nd
CD8a	146Nd
CD62L	147Sm
CD278	148Nd
CD5	149Sm
Ly6C	150Nd
CD25	151Eu
CD3e	152Sm
CD366	153Eu
CD152	154Sm
CD317	155Gd
CD223	156Gd
FoxP3	158Gd
Rorgt	159Tb
Tbet	160Gd
CD279	161Dy
KI-67	162Dy
Klrg1	163Dy
TIGIT	164Dy
MERTK	165Ho
CD26	166Er
F4/80	167Er
XCR1	168Er
TCRβ	169Tm
CD161	170Er
CD44	171Yb
Ly-6G	172Yb
CD172a	173Yb
MHCII	174Yb
NKG2a	175Lu
CD134	176Yb
CD45.2	198Pt
Cd11c	209Bi

differentiated T cells subsets (naïves and central memory (CM)) and tends to be less expressed on more differentiated subsets (effector memory (EM), EMRA[effector memory cells re-expressing CD45RA). Thus, HVEM expression was significantly upregulated on CD4$^+$ EM, but not other T cell subsets following activation. T cell proliferation and activation marked by the expression of CD25 significantly increased on anti-HVEM co-stimulation compared with control (figure 1E–H). Taken together,

Table 4 Flow cytometry panel for lymph node phenotyping

Marker	Fluorochrome
CD137	BUV395
DAPI	BUV496
CD11a	BUV737
CD49d	BUV805
CD122	BV421
CD27	BV510
CD69	BV605
CD44	BV650
CD8	BV711
CD5	FITC
CD3e	BB700
CD278	PE
CD25	PE-CF594
CD161	PE-Cy5
CD154	PE-Cy7
CD197	APC
CD62L	Alexa700
CD4	APC-Cy7

our results show that CIS-HVEM blockade enhances T cell activation.

HVEM expression is higher than PD-L1 in human lung and colorectal cancers

Next, we decided to study the expression status of HVEM on tumor from different cancers. Transcriptomic data from the TCGA containing 525 adenocarcinoma samples and 300 colorectal carcinoma samples were extracted, and the expression of HVEM and PD-L1 was examined (figure 2A,B). We found that HVEM was highly expressed in both cancers. While PD-L1 expression was high in lung cancer and low in colorectal cancers. Interestingly, HVEM expression is greater than that of PD-L1 expression in both cancers (figure 2A,B). Next, we studied HVEM and PD-L1 transcriptomic expression (from the cancer cell line encyclopedia) and cell surface expression by cytometry in lung and colorectal cancer cell lines (figure 2C,D). HVEM and PD-L1 are heterogeneously expressed in lung cancer cell lines, we selected two lung cancer cell lines that expressed both genes (NCIH2291) or in large majority HVEM compared with PD-L1 (NCIH2405) for subsequent experiments (figure 2C). The vast majority of colorectal cancer cell line highly expressed HVEM whereas PD-L1 was expressed in lower amount (figure 2D). Reflecting these observations, we selected HVEM$^+$PD-L1$^-$ HT29 cell line for subsequent experiments (figure 2D). These results were confirmed in NCIH2291 (HVEM$^+$ PD-L1$^+$), NCIH2405 (HVEM$^+$ PD-L1$^-$), and HT29 (HVEM+PD-L1$^-$) by flow cytometry assessment of PD-L1 and HVEM surface expression (figure 2E,F).

Anti-HVEM18-10 enhances T cells responses against lung cancer cell line NCIH2291

Knowing the expression of HVEM among tumor cell lines allowed us to further test anti-HVEM effect. Co-cultures of PBMCs and the lung cancer cell line NCIH2291 (HVEM$^+$ PD-L1$^+$) were performed during 72 hours in the presence of anti-CD3 in combination with an IgG1 control or anti-HVEM18-10. The addition of anti-HVEM18-10 to the co-culture drastically increased proliferation ratio and CD25 expression of CD4$^+$ and CD8$^+$ T cells compared with control (figure 3A–D). Moreover, the addition of anti-HVEM18-10 to the co-culture also drastically increased the amount of procytotoxic cytokines tumor necrosis factor (TNF)-α and interferon (IFN)-γ as measured by ELISA (figure 3E,F). These results confirm an effect of the blockade of HVEM on CIS-T cell activation and TRANS -activation as well.

Anti-HVEM18-10 triggers T cell activation, proliferation, and synergizes with anti-PD-L1

Anti-PD-L1 antibody has been a real game changer in IT to treat patients with lung cancer.[18] Therefore, we thought to test whether the combination of anti-HVEM18-10 to anti-PD-L1 could improve T cell responses in co-culture experiments with HVEM and PD-L1-positive lung tumor cell line. PBMCs were primed with suboptimal anti-CD3 dose, then activated with anti-HVEM18-10, anti-PD-L1, both antibodies (combo), or IgG1 control during 72 hours (figure 4A–D). The addition of anti-HVEM18-10 (blue bar) was sufficient to improve T cells proliferation and CD25 expression compared with control. Likewise, the anti-PD-L1 (red bar) also increased T cell activation and proliferation ratio compared with control. Interestingly, the combination of anti-HVEM18-10 and anti-PD-L1 (purple bar) in culture showed even greater effect on T cell proliferation and CD25 expression compared with the separate conditions. These results highlight the potential of anti-HVEM18-10 and anti-PD-L1 combination to strengthen T cell activation.

Interestingly, we next tested whether anti-HVEM18-10 could enhance T cell response against PD-L1$^-$ lung and colorectal cancer cell line (online supplemental figure 1). Anti-HVEM18-10 was sufficient to improve CD4$^+$ and CD8$^+$ T cell activation with a marked increase of CD25 expression and proliferation in co-culture with either lung or colorectal cell line, validating the use of anti-HVEM18-10 with PD-L1$^-$ tumors for future IT treatments.

huBTLA$^{+/+}$ and DKI mice show wild-type-like hematopoietic cell proportions

To test whether the effect of anti-HVEM18-10 in vivo occurs via CIS-blockade or TRANS-blockade using preclinical tumor models, we developed KI mice model expressing either huBTLA$^{+/+}$ or both huBTLA$^{+/+}$/huHVEM$^{+/+}$ or DKI (figure 5A). To produce huBTLA$^{+/+}$ mice, exon 2 from wild-type mouse was substituted by human exon 2. Likewise, HVEM$^{+/+}$ mice were developed by replacing exon 1 with human HVEM gene (tnfrsf14-001) exon 1. These mice were then crossed to obtain DKI mice. The presence of the insertion was confirmed by PCR and cytometry. The expression of
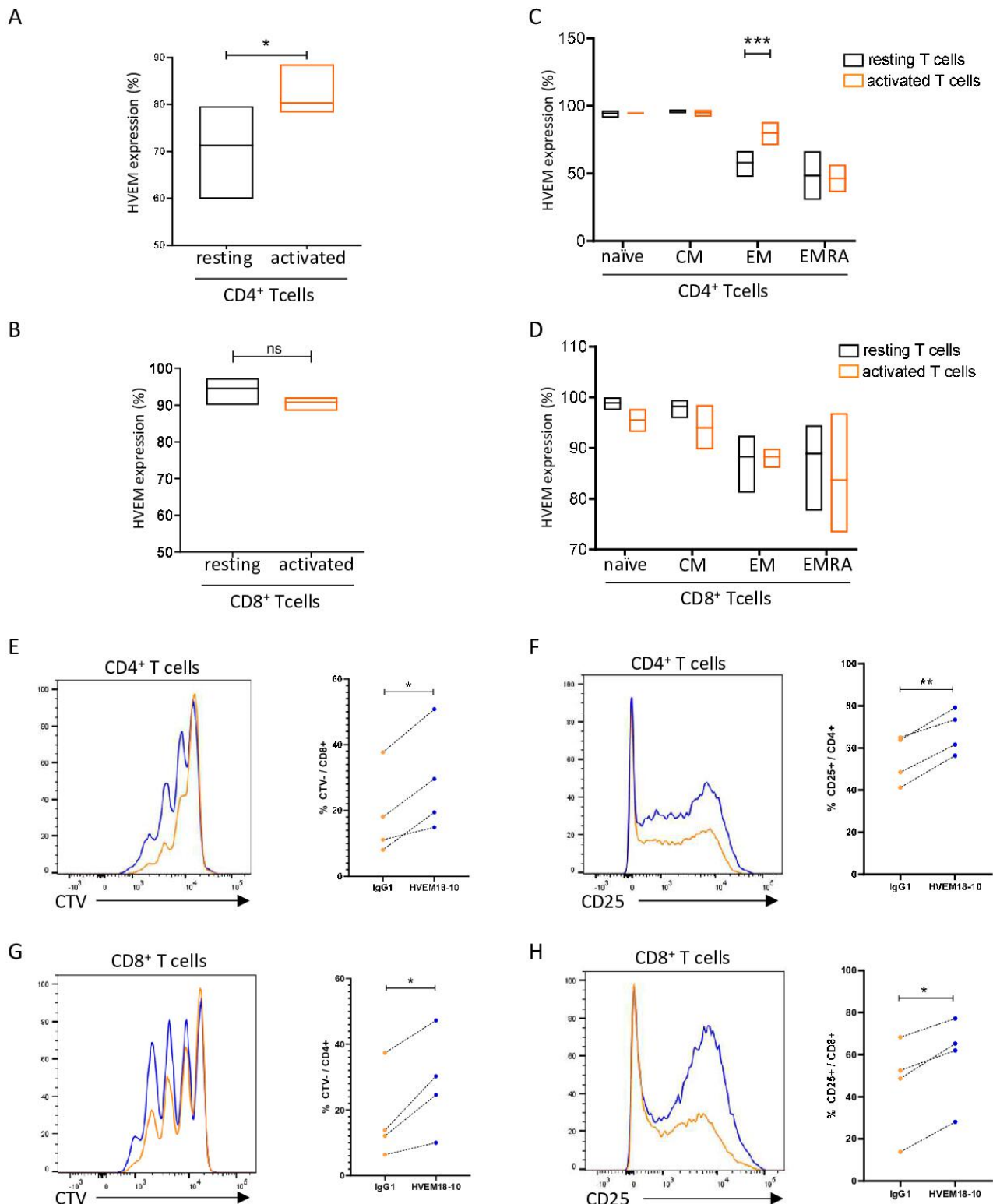
Figure 1 HVEM is highly expressed on T cells and the CIS-HVEM blockade enhance T cells activation. (A–H) Peripheral blood mononuclear cells (PBMCs) were isolated from healthy donors, and cultured for 72 hours with anti-CD3 (OKT3) stimulation alone (orange bars), with OKT3 stimulation and anti-HVEM18-10 treatment (blue bars/lines), or without any stimulation (black bars). HVEM expression was assessed in resting (black bars) and activated (orange bars) CD4$^+$ (A), CD4$^+$ T cells subsets (naïve, central memory (CM), effector memory (EM), and EMRA) (B), CD8$^+$ (C), CD8$^+$ T cells subsets (D) by flow cytometry on healthy donors (n=3). (E–H) PBMCs were incubated with OKT3 and anti-HVEM18-10 antibody (blue bars/lines) or a control monoclonal antibody (mAb) IgG1 (orange bars/lines). Proliferation profile of T cells was assessed by flow cytometry detecting Cell Trace Violet (CTV) (E, G for CD4$^+$ and CD8$^+$ T cells, respectively) or CD25 staining (F, H for CD4$^+$ and CD8$^+$ T cells, respectively). (E–H) One representative plot is shown for each T cell subset. Bar plots are the mean±SEM of four different healthy donor samples. (A–D n=3, E–H n=4). *P<0.05; **p<0.01; ***p<0.001 (Student's t-test). ns, not significant.
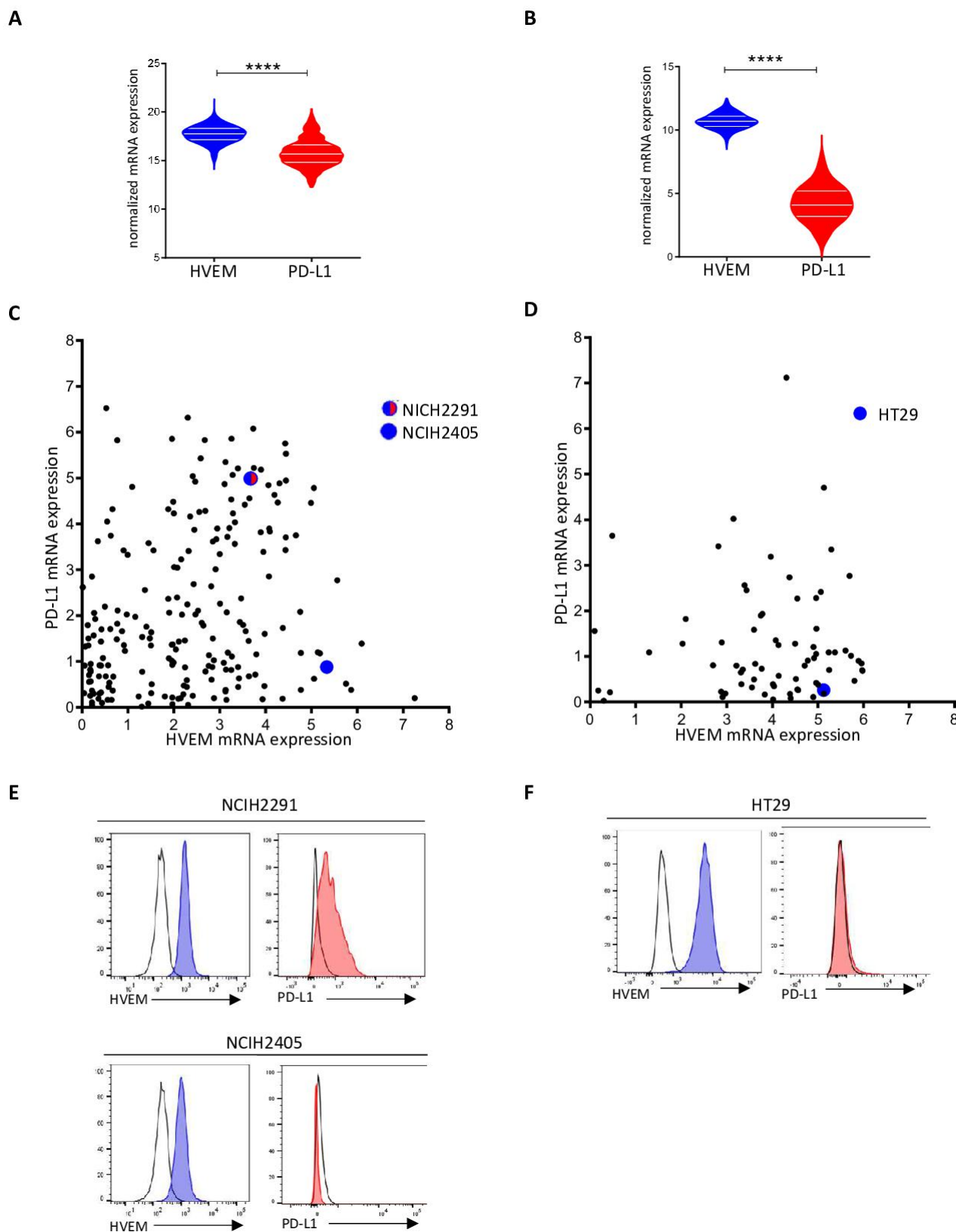
Figure 2 HVEM is more expressed than programmed death-ligand 1 (PD-L1) in lung and colorectal cancers. HVEM and PD-L1 transcriptomic expression was analyzed in 526 lung adenocarcinoma samples (A) and 388 colorectal carcinoma samples (B). Normalized expression data were extracted from The Cancer Genome Atlas (TCGA) database (****p<0.0001). HVEM and PD-L1 transcriptomic expression was analyzed in lung (C) and colorectal (D) cancer cell lines. (C, D) Data are extracted from the Cancer Cell Line Encyclopedia (CCLE) and expressed in log2(TPM+1). HVEM and PD-L1 phenotypic expression on selected lung (E) (NCIH2291 and NCIH2405, respectively) and colorectal (F) cancer cell line (HT29). HVEM staining in dark gray and control isotype in light gray. mRNA, messenger RNA.
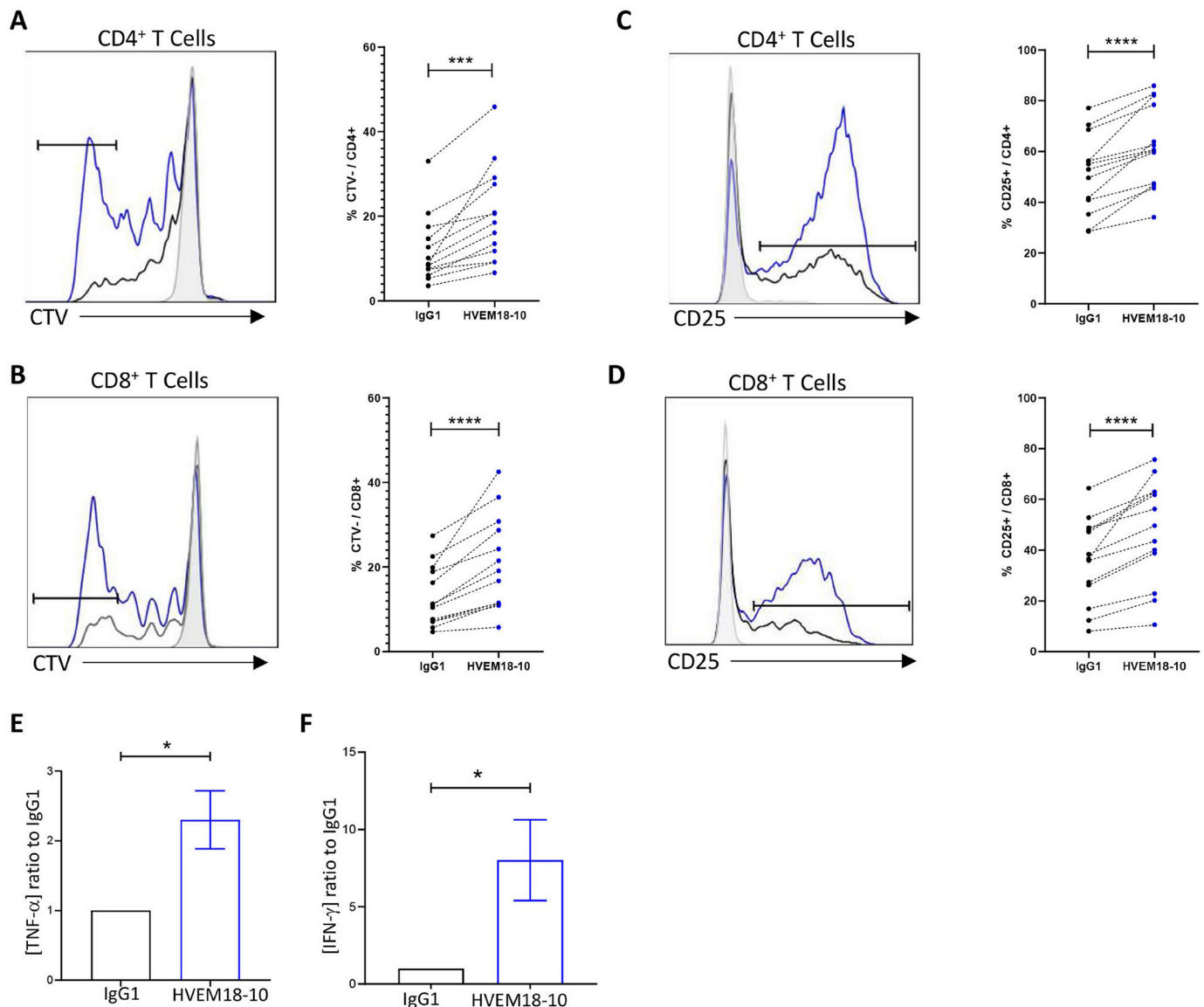
Figure 3 Anti-HVEM18-10 enhances T cells responses against NCIH2291. Adherent lung cancer cell line NCIH2291 was seeded in wells 24 hours before the experiment. Then we cultured peripheral blood mononuclear cells from healthy donors for 72 hours with OKT3 stimulation and treated or not with anti-HVEM18-10 antibody (blue bars/lines). (A–D) Proliferation profile of T cells by Cell Trace Violet (CTV) staining (A for CD4$^+$ and B for CD8$^+$ T cells) and CD25 expression (C for CD4$^+$ and D for CD8$^+$ T cells). (E, F) Tumor necrosis factor (TNF)-α (E) and interferon (IFN)-γ (F) secretion was measured by ELISA in culture supernatant. Bar plots are the mean±SEM of different healthy donor samples (A–D n=13; E–F n=10). *P<0.05; ***p<0.001; ****p<0.0001 (Student's t-test).

human/mouse HVEM on T cells, DC (dendritic cells), Ly6C$^+$ cells and neutrophil and BTLA on T cells and B cells was examined by cytometry (online supplemental figure 2A,B). Both HuBTLA$^{+/+}$ and DKI mice showed the same number of cells in the spleen (figure 5B) and same proportion of T cells by cytometry. Other lymphoid and myeloid cells are also found in the same proportions in both models (figure 5C). Indeed, the frequencies of B cells, $\gamma\delta$-Tcells and natural killer cells were similar among mice models. Similarly, myeloid cell frequencies (PMN[Polymorphonuclear], cDC1, cDC2, macrophages, monocytes) remained unchanged among these models (figure 5D). Gating strategies for different cells subset are shown in online supplemental figure 2C. These

observations allowed further in vivo tumor response studies with these new mouse models.

Blocking trans-BTLA-HVEM binding in vivo is sufficient to decrease solid tumor growth

We then decided to challenge huBTLA$^{+/+}$ mice with a colorectal cancer cell line MC-38 that is not expressing constitutively HVEM; 0.5×10^6 MC-38 tumor cells were injected subcutaneously in the right flank of huBTLA$^{+/+}$ mice. Mice bearing tumor between 50 and 100 mm^3 were then randomized at day 9 and mice were injected with anti-HVEM18-10 or isotype control every 3–4 days with for a total of six injections (online supplemental figure 3B).
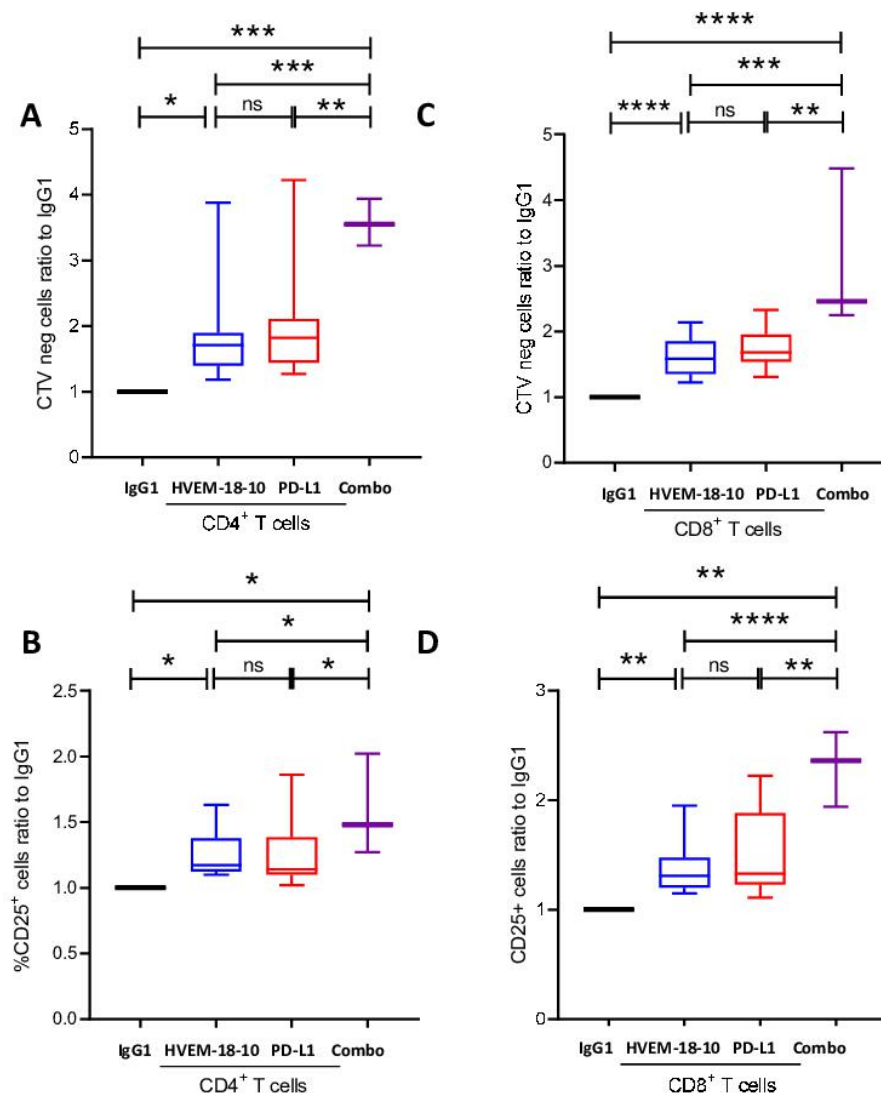
Figure 4 Anti-HVEM18-10 synergizes with anti-programmed death-ligand 1 (PD-L1) to enhance T cells responses against lung cancer cell line NCIH2291. Adherent lung cancer cell line NCIH2291 were cultured with peripheral blood mononuclear cells from healthy donors for 72 hours with CD3 stimulation and treated with anti-HVEM18-10 antibody (blue bars/lines) or not (black bars/line) (A–D) proliferation profile of T cells by Cell Trace Violet (CTV) staining (A for CD4$^+$ and C for CD8$^+$ T cells) and CD25 expression (B for CD4$^+$ and D for CD8$^+$ T cells). Bar plots are the mean±SEM of different healthy donors samples (n=13 for IgG1, anti-HVEM, and anti-PD-L1 conditions, n=3 for combo condition). *P<0.05; **p<0.01; ***p<0.001; ****p<0.0001 (Student's t-test). ns, not significant.

As envisioned, tumor growth of parental MC-38 (HVEM⁻) injected with an isotype control or with anti-HVEM18-10 at 10 mg/kg did not show any significant decrease in tumor growth. We then transduced huHVEM in MC-38 cells and selected a clone that that was able to bind effectively anti-HVEM18-10 (namely: MC-38^{huHVEM}; online supplemental figure 3A). MC-38^{huHVEM} tumor cells were injected subcutaneously as previously described. Here, we observed a decrease in tumor growth at any dose of anti-HVEM18-10 used 2 and 10 mg/kg (figure 6B; online supplemental figure 3C). Moreover, 2 mice out of 10 in the 2 mg/kg dose and 1 out of 10 in the 10 mg/kg dose fully rejected the tumors. These three tumor free mice were rechallenged with fourfold more concentrated MC-38^{huHVEM} tumors cell inoculate (ie, $2×10^6$ cells) in contralateral flank. All animals were monitored during

21 days postchallenge to ensure immunological memory persistence. In two of these three mice, the tumor was not measurable at day 21. However, after the euthanasia of these three mice at day 21, tumor mass was absent in their left flank revealing the presence of a scar tissue instead (figure 6C). Altogether, these data confirmed the in vivo efficiency of anti-HVEM18-10 to block trans-BTLA-HVEM binding.

Anti-HVEM treatment decreases tumor growth, exhausted CD8$^+$ T cell, KLRG1⁻ regulatory T cell infiltrate and increases EM conventional CD4$^+$ T cell infiltrate

Then, we investigated the effect of anti-HVEM on DKI lymphocytes (figure 7A). The proliferation of sorted spleen T cells was assessed after 72 hours of stimulations with coated anti-CD3 and anti-HVEM18-10 or isotype
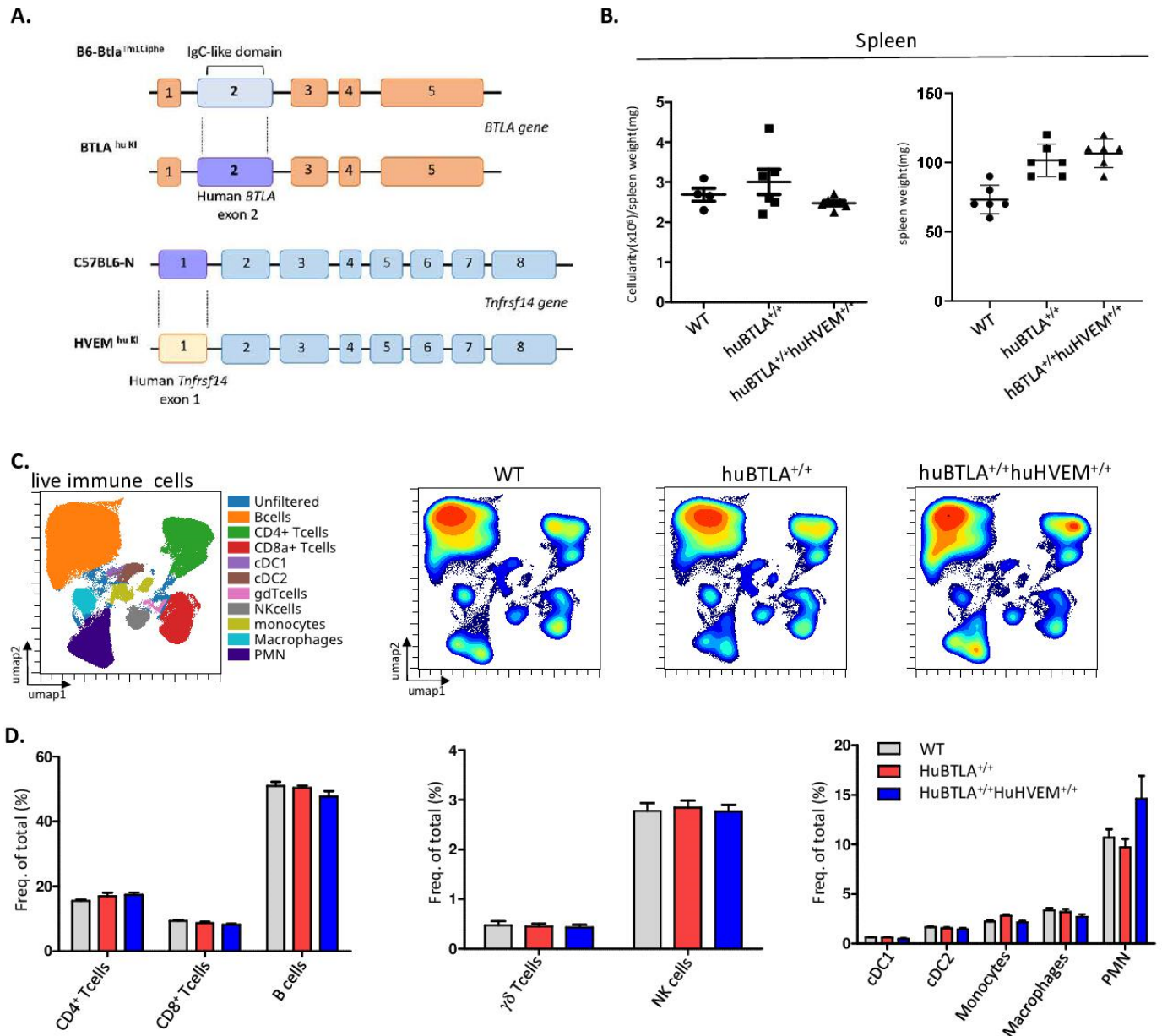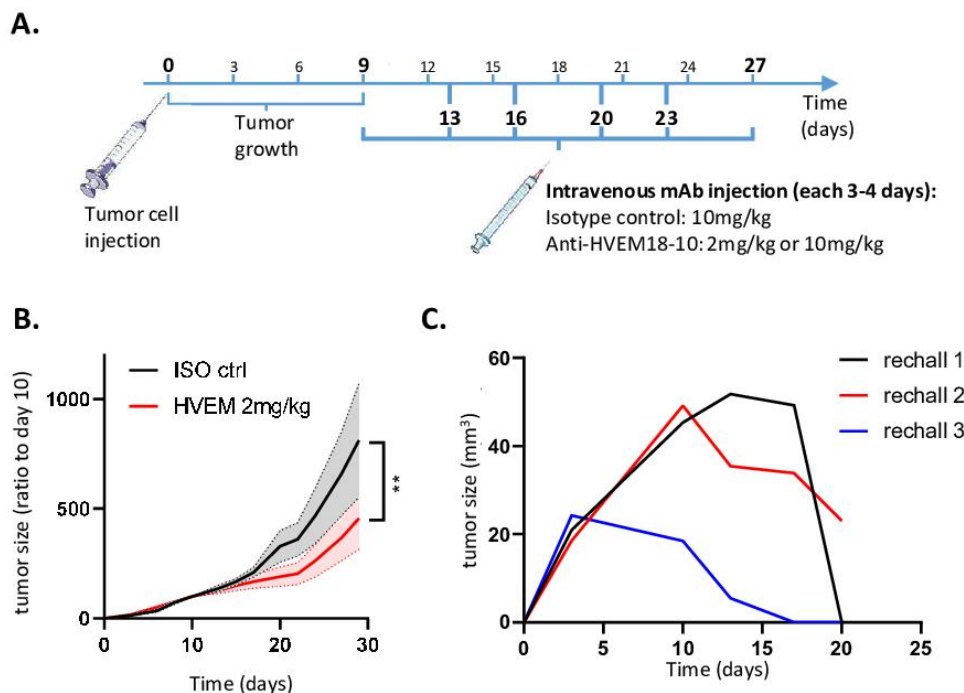
Figure 5 Human (hu) B and T lymphocyte attenuator (BTLA) and double knockin (DKI) mice show the same hematopoietics cell homeostasis. (A) Representative scheme of huBTLA$^{+/+}$huBTLA$^{+/+}$ and huHVEM$^{+/+}$ genetic modification. For huBTLA$^{+/+}$huBTLA$^{+/+}$, murine exon 2 was replaced by huBTLA exon 2 and for huHVEM$^{+/+}$ murine exon 1 was replaced by huHVEM gene exon 1. (B) Numbers of total cell per spleen weight for wild-type (WT), huBTLA$^{+/+}$huBTLA$^{+/+}$, and huHVEM$^{+/+}$ is represented (left) spleen weight (mg) is represented on the right for six control (Ctrl), huBTLA$^{+/+}$, and six huHVEM$^{+/+}$huBTLA$^{+/+}$ mice. (C) uniform manifold approximation and projection (UMAP) showing the distribution of immune cell subset within WT, huBTLA, and DKI mice. (D) Immune cell subset frequency was quantified in the three mice groups. Density UMAP representing major and minor cell subsets (bottom). NK, naturak killer.

control at increasing concentration. The addition of anti-HVEM18-10 increased DKI T cells proliferation in a dose-dependent manner similarly to human T cells (figure 1), validating in vitro this new mouse model (figure 7A). The effect of anti-HVEM18-10 in vivo was then studied using DKI mice. DKI mice were challenged with 0.5×10^6 MC-38^{huHVEM} tumor cells which were injected subcutaneously as described previously. We observed a decrease in tumor growth when anti-HVEM18-10 was injected at 2 mg/kg (figure 7B). Moreover, 3 mice out of 12 in the

anti-HVEM18-10 group completely rejected the tumors and were later investigated in rechallenge experiments. To understand the immune mechanisms underlying tumor reduction after anti-HVEM18-10 treatment, tumor infiltrating lymphocytes (TILs) phenotypes were investigated in anti-HVEM18-10-treated mice and isotype controls by mass cytometry. Tumor infiltrating T cells was mapped using UMAPs in anti-HVEM18-10 and isotype controls treated mice. Density analysis of UMAPs showed phenotypic variations between conditions (figure 7C),

Figure 6 Blocking trans-B and T lymphocyte attenuator (BTLA)-HVEM binding in vivo is sufficient to decrease solid tumor growth. (A) Scheme representing in vivo tumor experiments settings. (B) Measure of tumor growth showed as ratio to size of tumor at randomization day. Colorectal cancer cells MC-38^huHVEM were injected (0.5×10^6) at day 0 in human (hu)BTLA^+/+ mice and isotype (ISO) control (ctrl) (black) or anti-HVEM18-10 antibody at 2 mg/kg (red) concentration were injected. (C) Tumor-free mice from B and C measure of tumor growth after MC-38^huHVEM tumor cells rechallenge (2×10^6). (B–C) n≥7; (D) n=3. **p<0.01 (two-way analysis of variance). mAb, monoclonal antibody.

that were investigated by unsupervised analysis using T cell subset markers (online supplemental figure 4A–C). Next, a clustering of tumor infiltrating T cells was performed using the well-described PhenoGraph algorithm and the 19 identified clusters were projected on the UMAP highlighting the heterogeneity of intratumoral T cells. Five clusters belonging to regulatory T (Treg) cells (CD4^+CD25^+FoxP3^+), eight clusters belonging to conventional CD4^+ T cells (conv. CD4^+ T cells/non-Tregs) and six clusters belonging to CD8^+ T cells were identified (figure 7D,E). Interestingly, while T cell clusters were very heterogeneous, only three clusters were significantly altered in anti-HVEM18-10 compared with isotype control treated mice (figure 7E–H and online supplemental figure 4B). These clusters were manually gated for validation in online supplemental figure 4D,E. First, cluster 13, a subset of KLRG1^-CTLA-4^+Ki67^+ Tregs, was statistically decreased in anti-HVEM18-10 condition (figure 7F and online supplemental figure 4E). Cluster 11, composed of EM, CD44^+CD62L^- CD4^+ conv. T cells, was significantly increased under anti-HVEM18-10 treatment (figure 7G and online supplemental figure 4E). In this cluster, EM CD4^+ T cells did not exhibit marks of immunosuppression or exhaustion such as high levels of PD-1, TIM-3, or T cell immunoreceptor with Ig and ITIM domains (TIGIT). Therefore, these EM CD4^+ T cells may favor antitumoral immune response. Third, cluster 17, an EM (CD44^+CD62L^-) CD8^+ T cell subsets showed higher expression of PD-1 and expressed T-cell

immunoglobulin and mucin containing protein-3 (TIM-3), Lymphocyte-activation gene 3 (LAG-3), and CTLA-4. Therefore, we labeled these EM CD8^+ T cells as exhausted. Interestingly, these exhausted CD8^+ T cells decreased under anti-HVEM18-10 treatment (figure 7H and online supplemental figure 4E). Taken together, our results demonstrate a loss in immunosuppressive T cell subsets (KLRG1^- Tregs, and exhausted EM CD8^+ T cells) and an increase in EM CD4^+ T cells. These phenotypic changes contribute to the reduction of tumor growth and correspond to phenotypes observed in previous studies showing tumor reduction following immunotherapeutic treatments in mouse models.[19 20]

Anti-HVEM-therapy builds a tumor-specific memory T cell response associated with tumor antigen responsive T cells

We next decided to compare in vivo the effect of anti-HVEM response to a well-known checkpoint inhibitor anti-CTLA-4 on tumor growth and T cell activation. DKI mice were challenged with 2×10^6 MC-38^huHVEM tumor cells as previously described, then injected with an isotype control, anti-HVEM18-10 (2 mg/kg), or anti-CTLA-4 (2 mg/kg) at days 7 and 10. Tumor infiltrating and draining lymph node (LN) T cell phenotype was analyzed at day 14. As expected, the injection of anti-HVEM18-10 or anti-CTLA-4 decreased tumor growth and led to total tumor rejection in three mice under anti-HVEM and anti-CTLA-4 treatment (figure 8A and online supplemental figures 5A–C). Hence, tumor-free mice respectively from
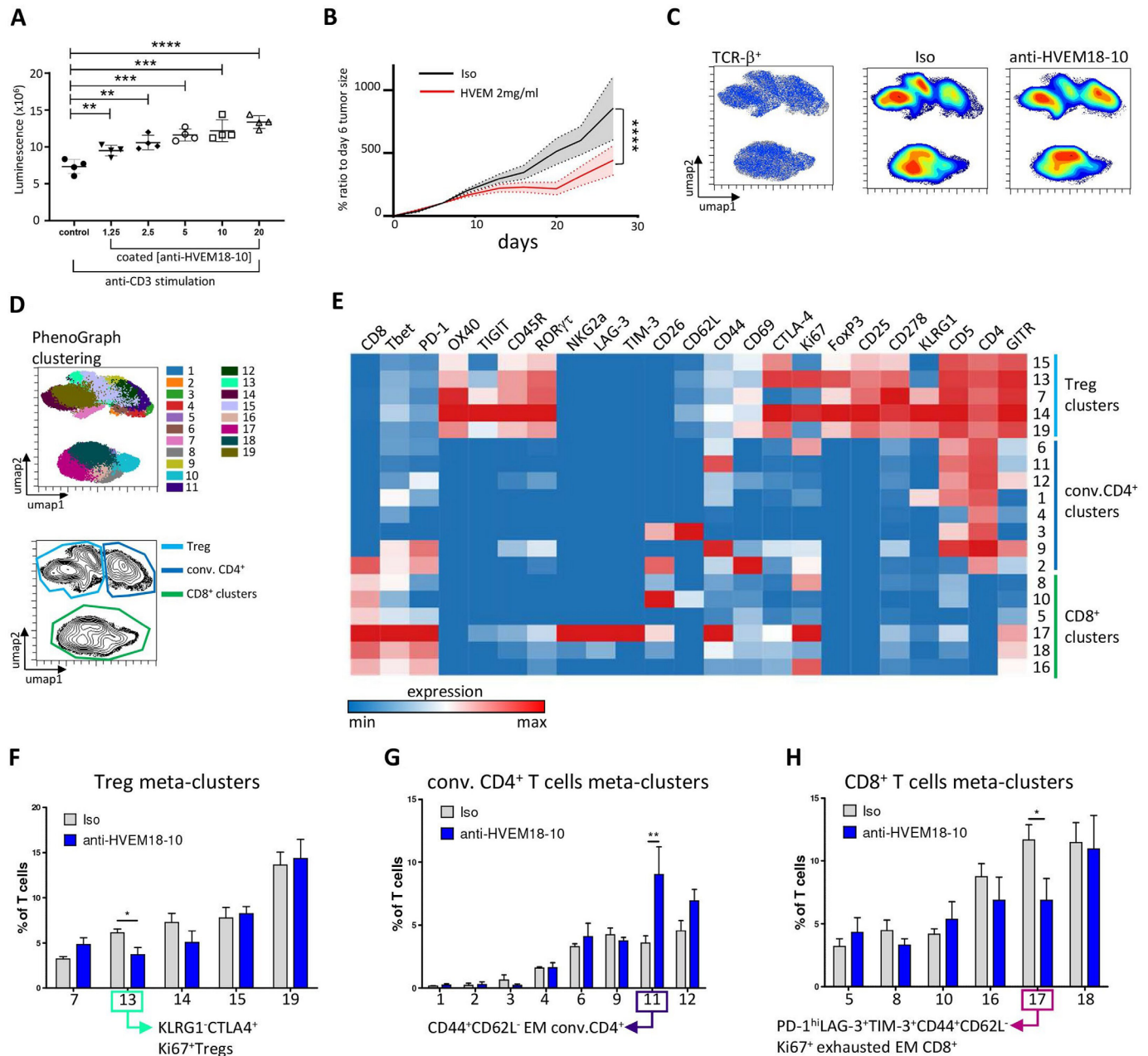
Figure 7 Anti-HVEM treatment decreases tumor growth, exhausted CD8+ T cell, KLRG1- regulatory T (Treg) cells infiltrate, and increases effector memory (EM) conventional (conv.) CD4+ T cell infiltrate. (A) T cells from double knockin (DKI) mice or wild-type (WT) were cultured with CD3 alone or with anti-HVEM18-10 at increasing concentration. T cells proliferation assessed by luminescence using Cell titerglo. (B) Measure of tumor growth showed as ratio to size of tumor at randomization day. Colorectal cancer cells MC-38^huHVEM were injected (0.5×10^6) at day 0, and isotype control (Iso ctrl) (black) or anti-HVEM18-10 antibody at 2 mg/kg (blue) concentration were injected. (C) UMAP analysis of anti-HVEM18-10 (blue) or Iso ctrl (Iso, gray). Density analysis revealed phenotypic modification between anti-HVEM treatment and Isotype treatment. (D) PhenoGraph clustering was performed on tumor infiltrating lymphocytes (TILs) from anti-HVEM18-10 and Iso ctrl-treated mice and represented as a UMAP. Nineteen meta-clusters were identified among T cells (top). Treg (light blue), conv. CD4+ T cell (dark blue), and CD8+ T cell (green) cluster gating on a UMAP (bottom). (E) Heatmap representation of marker expression among the 19 identified PhenoGraph meta-clusters. Cluster were associated with Tregs (light blue), conv. CD4+ T cells (dark blue), and CD8+ T cells (green). Bar charts represent cluster variation between anti-HVEM18-10 treatment compared with Iso ctrl in Tregs (F), conv. CD4+ T cells (G), and CD8+ T cells (H). *P<0.05; **p<0.01; ***p<0.001; ****p<0.0001.

anti-HVEM and anti-CTLA-4 treatment were rechallenged with 6×10^6 cells MC-38^huHVEM tumors cells in contralateral flank. Interestingly, tumors did not grow in these mice 14 days after rechallenge. Therefore, we

hypothesized that primary tumor rejection built an anti-tumor T cell memory response that led to rechallenge rejection. Hence, we compared T cell response in rechallenged mice following anti-HVEM18-10 and anti-CTLA-4
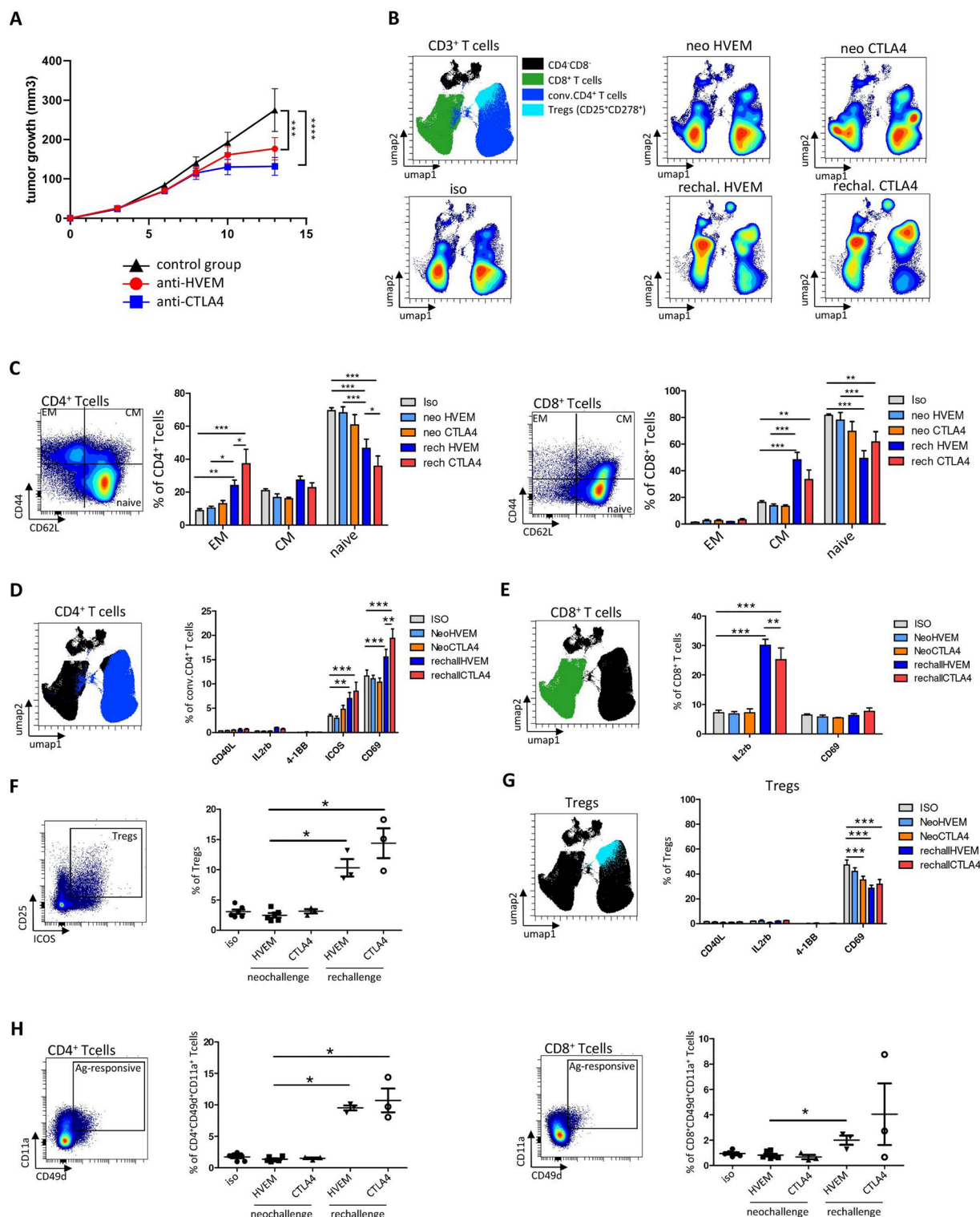
Figure 8 Anti-HVEM18-10 therapy builds a memory T cell response associated with CD4+ and CD8+ tumor antigen responsive T cells. (A) Tumor growth profile overtime following, isotype control (black), anti-CTLA-4 (blue), or anti-HVEM18-10 (red) treatment. (B) Lymph nodes (LN) were dissociated and cell stained for flow cytometry. UMAPs represent the phenotypic distribution of T cells within LN in isotype control mice (n=6), anti-HVEM18-10 (n=6), or anti-CTLA-4 (n=3) treated neo-challenged mice or anti-HVEM18-10 (n=3) or anti-CTLA-4 treated rechallenged mice (n=3). (C) Study of effector memory (EM), central memory (CM), and naïve conventional (conv.) CD4+ and CD8+ T cells among neo-challenged and rechallenged conditions (D) Study of immune checkpoint expression in conv. CD4+ T cells among neo-challenged and rechallenged conditions. (E) Study of immune checkpoint expression in CD8+ T cells among neo-challenged and rechallenged conditions. (F) Regulatory T (Treg) cells frequency among neo-challenged and rechallenged conditions. (G) Study of immune checkpoint expression in Tregs among neo-challenged and rechallenged conditions. (H) Study of CD49d+CD11a+ tumor-specific CD4+ and CD8+ T cells in neo-challenged and rechallenged conditions. *P<0.05; **p<0.01; ***p<0.001.

treatments. Draining LN were resected and dissociated then T cell phenotypes were assessed by flow cytometry. T cell mapping was drastically modified after rechallenge compared with neo-challenge as shown by density UMAPs (figure 8B). Then, memory T cell subsets were gated (using CD44 and CD62L expression) and neo-challenged and rechallenged mice treated with anti-HVEM or anti-CTLA-4 were compared. We found that rechallenged treated mice either for anti-HVEM18-10 or anti-CTLA-4 were enriched in EM CD4$^+$ T cells (CD44$^+$CD62-L$^-$) compared with their neo-challenged counterpart and isotype control (figure 8C, left). This increase was significantly superior in rechallenged CTLA-4-treated compared with rechallenged HVEM-treated mice (figure 8C, left). Noteworthy, naïve CD4$^+$ T cells decreased after rechallenge. Concerning CD8$^+$ T cells, we found that rechallenged mice with anti-HVEM18-10 or anti-CTLA-4 showed more CM CD8$^+$ T cells (CD44$^+$CD62-L$^+$) compared with their neo-challenged counterpart and isotype control (figure 8C, right and online supplemental figure 5D). This increase tended to be superior in rechallenged HVEM-treated compared with rechallenged CTLA-4-treated mice. Again, naïve CD8$^+$ T cells decreased as well on treatments. Taken together, these results show an enrichment in memory CD8$^+$ and CD4$^+$ T cells in rechallenged conditions.

Next, we investigated activation marker expression on CD4$^+$ and CD8$^+$ T cells from LN (figure 8D,E and online supplemental figure 5E). In CD4$^+$ T cells no modification in the expression of CD40L, IL-2Rβ, or 4-1BB was observed. However, the expression of inducible costimulator (ICOS) in rechallenged mice after anti-HVEM18-10 or anti-CTLA-4 treatment increased compared with controls. Similarly, CD69$^+$CD4$^+$ T cells were more abundant in rechallenged mice compared with controls. Noteworthy, CD69 overexpression was greater in anti-CTLA4 rechallenged mice compared with anti-HVEM rechallenged mice (figure 8D). In CD8$^+$ T cells, an overexpression of IL2-Rβ in rechallenged mice compared with controls was observed. Here, IL2-Rβ expression was greater in anti-HVEM18-10 rechallenged mice compared with anti-CTLA-4 rechallenged mice (figure 8E). This suggests a better response to IL-2 or IL-15 and consequently more CD8$^+$ T cell activation. Noteworthy, we did not notice any difference in the expression of CD69 on CD8$^+$ T cells (figure 8E). Next, the Treg population within LNs after rechallenge was investigated. Treg frequency increased after rechallenge in both anti-HVEM18-10 and anti-CTLA-4 mice compared with anti-HVEM18-10 neo-challenged group (figure 8F). Last, a decrease in the expression of CD69 in Treg was observed, suggesting less activation or recruitment of peripheral blood Treg (figure 8G). Taken together, these results show that rechallenged mice rejected secondary tumor inoculation thanks to a strong T cell memory response linked to an increased expression of IL-2Rβ and a recruitment of tumor responsive CD8$^+$ and CD4$^+$ T cells.

Recently, the CD11a$^+$CD49d$^+$ CD4$^+$ and CD8$^+$ T cells were reported as tumor antigen responsive T cells, which participate to antitumor response.[21] Therefore, we gated CD11a$^+$CD49d$^+$ CD4$^+$ and CD8$^+$ T cells (figure 8D and online supplemental figure 5F) and showed that tumor antigen responsive CD4$^+$ T cells increased on rechallenge with anti-HVEM18-10 and anti-CTLA-4 mice (figure 8H) compared with controls. Interestingly, tumor antigen responsive CD8$^+$ T cells significantly increased after rechallenge with anti-HVEM18-10 only (figure 8H). Taken together, our results show that the antitumoral memory response that allowed tumor rejection relies on enrichment in CD4$^+$ and CD8$^+$ memory subpopulations, increase of IL-2Rβ/activation markers, and more importantly on tumor antigen-specific T cell subsets, which most likely allow secondary tumor rejection.

DISCUSSION

HVEM is a molecular switch as its effect depends on the ligand involved that is largely expressed in lung and colorectal tumors. Here, we showed that anti-HVEM18-10 antagonist mAb potentiates in vitro T cell proliferation and activation by blocking preferentially the interaction with the inhibitory ligands of HVEM. Then, we developed an innovative mouse model expressing both human BTLA and human HVEM. Anti-HVEM18-10 injection in mice induced the development of a marked T cell-memory phenotype and tumor antigen-specific (CD49d$^+$CD11a$^+$) T cells contributing in HVEM$^+$ tumor reduction or rejection, especially after rechallenge. Therefore, HVEM targeting is a great addition to the currently available arsenal of IT.

To assess the clinical relevance of HVEM targeting in lung and colorectal tumors, we screened HVEM expression public transcriptomic databases. We found that HVEM was largely expressed in these cancers and did not correlate with PD-L1 expression. Surprisingly, the literature reporting HVEM expression in lung and colorectal cancers remains sparse.[8 14 22] A more detailed multiparametric study, like was shown for pancreatic cancer[23] would participate to the improvement of tumor type stratification and define who could benefit from HVEM18-10 mAb treatment.

In our in vitro preclinical settings, we showed that the anti-HVEM18-10 mAb increased primary human αβ-T cells activity alone (CIS-activity) or in presence of HVEM-expressing lung or colorectal cancer cells in vitro (TRANS-activity). Thus, we observed an immune reactivation similarly to that triggered by anti-PD-1 or anti-CTLA-4 treatment, favoring the idea that HVEM18-10 mAb avoids HVEM interaction with its inhibitory ligands. Indeed, our model do not allow to appreciate fully the effect of the binding of HVEM18-10 mAb on huCD160 and huLIGHT interaction with HVEM. The same observation was made with anti-HVEM18-10, which allowed γδ-T cells activation, especially against HVEM$^+$ lymphoma cells.[15] In the light of these observations,

the use of HVEM18-10 mAb to potentiate anti-tumor T cell responses in hematological cancer as well as in solid cancers is of great interest.

Interestingly, anti-HVEM18-10 synergized with anti-PD-L1 effects and maximized T cells responses when tumor cells expressed both targets. Therefore, anti-HVEM18-10 could be used in combination with other ICI therapies and reinforce the still growing arsenal of ICI combinations in ongoing trials anti-CTLA4/anti-PD-L1[24] anti-TIGIT/anti-PD-L1,[25] and anti-BTN3A1/anti-PD-L1.[26] Nevertheless, we showed that anti-HVEM18-10 alone is still sufficient to trigger efficient T cells responses in PD-L1$^-$ conditions. Thus, anti-HVEM18-10 may increase the target patient population independently of their PD-L1 status and PD-L1$^-$ cancers such as colorectal cancer may benefit from this new treatment.

Recently, anti-HVEM IT was investigated in a prostate cancer mouse model,[27] where Aubert et al showed that anti-HVEM18-10 reduced the growth of a HVEM$^+$ tumors in NOD.SCID.gc-null mice reconstituted with human T cells. In our study, we generated innovative immunocompetent mouse models expressing extracellular domains of huBTLA or both huBTLA and huHVEM. This, allowed preclinical experiments settings using human anti-HVEM18-10 in immunocompetent mice bypassing the use of human T cell reconstitution in nude mice. TIL phenotype showed a decrease in Treg infiltration, CD8$^+$ T cells exhaustion, and an increase of EM CD4$^+$ T cells, expanding results from Aubert et al in prostate tumors[27] to colon cancer. In addition, anti-CTLA4 treatment showed similar phenotypic modifications, which was already reported in the literature.[19 20] Our new mouse models allowed the study of therapeutic mAb directly in an immunocompetent and dynamic environment. To date, only one recent study described a KI mouse model expressing human PD-1 and CTLA-4 molecules.[28] The number of these syngeneic mouse models will increase in the future being closer to the clinic.

In our settings, around 20% of the mice completely rejected the tumor enabling the study of memory response induced by the rechallenge. Within tumor draining LN, we found a specific T cell memory composition, marked by an increase in IL-2Rβ$^+$ CM CD8$^+$ T cells and EM CD4$^+$ T cells in comparison to neo-challenged mice. More importantly, draining LN sheltered a population of CD49d$^+$CD11a$^+$ CD8$^+$ and CD4$^+$ lymphocytes, which were recently described as tumor antigen-specific T cells.[29] In a previous collaborative study, we showed that the addition of anti-HVEM18-10 was sufficient to decrease prostate cancer tumor growth and this effect was reverted by CD8 depletion.[27] Thus, the antitumoral effect triggered by anti-HVEM18-10 is mainly due to CD8$^+$ T cells. Therefore, anti-HVEM18-10 treatment leads to a systemic, tumor antigen-specific, T cell memory response allowing the mice to control distal secondary tumor implantation, similar to CTLA4 or anti-PD-1 treatment in other studies.[30–33]

CONCLUSION

HVEM appears to be a very promising IT target for oncological and hematological malignancies. Anti-HVEM18-10 mAb treatment demonstrated that antitumor immune response was strengthened, delays tumor growth or eradicate tumors, and induces a memory immune response in a cutting-edge preclinical mouse model. Altogether, these results highlight the interest of anti-HVEM IT alone or in combination with another IT to further enhance anti-tumor immunity.

Author affiliations
^{1}Department of Immunomonitoring, Institut Paoli-Calmettes, Marseille, France
^{2}Team Immunity and Cancer, Centre de Recherche en Cancérologie de Marseille, Marseille, France
^{3}Centre d'Immunophénomique—CIPHE (PHENOMIN), Marseille, France
^{4}Aix-Marseille University, Marseille, France
^{5}Department of Multidisciplinary Oncology and Therapeutic Innovations, CHU NORD, Marseille, France

ORCID iDs
Laurent Gorvel http://orcid.org/0000-0001-7526-261X
Frédéric Fiore http://orcid.org/0000-0001-7955-6594
Jacques A Nunes http://orcid.org/0000-0003-4865-0400
Geoffrey Guittard http://orcid.org/0000-0002-6061-8553
Daniel Olive http://orcid.org/0000-0003-1299-4113

REFERENCES

1. Garon EB, Rizvi NA, Hui R, *et al*. Pembrolizumab for the treatment of non-small-cell lung cancer. *N Engl J Med* 2015;372:2018–28.
2. Fehrenbacher L, Spira A, Ballinger M, *et al*. Atezolizumab versus docetaxel for patients with previously treated non-small-cell lung cancer (poplar): a multicentre, open-label, phase 2 randomised controlled trial. *Lancet* 2016;387:1837–46.
3. André T, Shiu K-K, Kim TW, *et al*. Pembrolizumab in microsatellite-instability-high advanced colorectal cancer. *N Engl J Med* 2020;383:2207–18.
4. Oh CR, Kim JE, Hong YS, *et al*. Phase II study of durvalumab monotherapy in patients with previously treated microsatellite instability-high/mismatch repair-deficient or POLE-mutated metastatic or unresectable colorectal cancer. *Int J Cancer* 2022;150:2038–45.
5. Montgomery RI, Warner MS, Lum BJ, *et al*. Herpes simplex virus-1 entry into cells mediated by a novel member of the TNF/NGF receptor family. *Cell* 1996;87:427–36.
6. Murphy KM, Nelson CA, Sedý JR. Balancing co-stimulation and inhibition with BTLA and HVEM. *Nat Rev Immunol* 2006;6:671–81.
7. Malissen N, Macagno N, Granjeaud S, *et al*. HVEM has a broader expression than PD-L1 and constitutes a negative prognostic marker and potential treatment target for melanoma. *Oncoimmunology* 2019;8:e1665976.
8. Inoue T, Sho M, Yasuda S, *et al*. HVEM expression contributes to tumor progression and prognosis in human colorectal cancer. *Anticancer Res* 2015;35:1361–7.
9. Lan X, Li S, Gao H, *et al*. Increased BTLA and HVEM in gastric cancer are associated with progression and poor prognosis. *Onco Targets Ther* 2017;10:919–26.
10. Tsang JYS, Chan K-W, Ni Y-B, *et al*. Expression and clinical significance of herpes virus entry mediator (HVEM) in breast cancer. *Ann Surg Oncol* 2017;24:4042–50.
11. Cai G, Freeman GJ. The CD160, BTLA, LIGHT/HVEM pathway: a bidirectional switch regulating T-cell activation. *Immunol Rev* 2009;229:244–58.
12. Watanabe N, Gavrieli M, Sedy JR, *et al*. Btla is a lymphocyte inhibitory receptor with similarities to CTLA-4 and PD-1. *Nat Immunol* 2003;4:670–9.
13. Demerlé C, Gorvel L, Olive D. Btla-Hvem couple in health and diseases: insights for immunotherapy in lung cancer. *Front Oncol* 2021;11:682007.
14. Ren S, Tian Q, Amar N, *et al*. The immune checkpoint, HVEM may contribute to immune escape in non-small cell lung cancer lacking PD-L1 expression. *Lung Cancer* 2018;125:115–20.
15. Gertner-Dardenne J, Fauriat C, Orlanducci F, *et al*. The co-receptor BTLA negatively regulates human Vγ9Vδ2 T-cell proliferation: a potential way of immune escape for lymphoma cells. *Blood* 2013;122:922–31.
16. Bian B, Fanale D, Dusetti N, *et al*. Prognostic significance of circulating PD-1, PD-L1, pan-btn3as, BTN3A1 and BTLA in patients with pancreatic adenocarcinoma. *Oncoimmunology* 2019;8:e1561120.
17. Yiu G, Rasmussen TK, Tsai BL, *et al*. High interferon signature leads to increased STAT1/3/5 phosphorylation in PBMCs from SLE patients by single cell mass cytometry. *Front Immunol* 2022;13:833636.
18. Herbst RS, Giaccone G, de Marinis F, *et al*. Atezolizumab for first-line treatment of PD-L1–selected patients with NSCLC. *N Engl J Med* 2020;383:1328–39.
19. Wei SC, Levine JH, Cogdill AP, *et al*. Distinct cellular mechanisms underlie anti-CTLA-4 and anti-PD-1 checkpoint blockade. *Cell* 2017;170:1120–33.
20. Wei SC, Anang N-AAS, Sharma R, *et al*. Combination anti–CTLA-4 plus anti–PD-1 checkpoint blockade utilizes cellular mechanisms partially distinct from monotherapies. *Proc Natl Acad Sci USA* 2019;116:22699–709.
21. McDermott DS, Varga SM. Quantifying antigen-specific CD4 T cells during a viral infection: CD4 T cell responses are larger than we think. *The Journal of Immunology* 2011;187:5568–76.
22. Sasaki Y, Hokuto D, Inoue T, *et al*. Significance of herpesvirus entry mediator expression in human colorectal liver metastasis. *Ann Surg Oncol* 2019;26:3982–9.
23. Steele NG, Carpenter ES, Kemp SB, *et al*. n.d. Multimodal mapping of the tumor and peripheral blood immune landscape in human pancreatic cancer. *Nat Cancer*;1:1097–112.
24. Meric-Bernstam F, Larkin J, Tabernero J, *et al*. Enhancing anti-tumour efficacy with immunotherapy combinations. *Lancet* 2021;397:1010–22.
25. Cho BC, Abreu DR, Hussein M, *et al*. Tiragolumab plus atezolizumab versus placebo plus atezolizumab as a first-line treatment for PD-L1-selected non-small-cell lung cancer (CITYSCAPE): primary and follow-up analyses of a randomised, double-blind, phase 2 study. *Lancet Oncol* 2022;23:781–92.
26. De Gassart A, Le K-S, Brune P, *et al*. Development of ICT01, a first-in-class, anti-BTN3A antibody for activating Vγ9Vδ2 T cell-mediated antitumor immune response. *Sci Transl Med* 2021;13:eabj0835.
27. Aubert N, Brunel S, Olive D, *et al*. Blockade of HVEM for prostate cancer immunotherapy in humanized mice. *Cancers (Basel)* 2021;13:3009.
28. Dovedi SJ, Elder MJ, Yang C, *et al*. Design and efficacy of a monovalent bispecific PD-1/CTLA4 antibody that enhances CTLA4 blockade on PD-1+ activated T cells. *Cancer Discov* 2021;11:1100–17.
29. Christiaansen AF, Dixit UG, Coler RN, *et al*. Cd11A and cd49d enhance the detection of antigen-specific T cells following human vaccination. *Vaccine* 2017;35:4255–61.
30. Pedicord VA, Montalvo W, Leiner IM, *et al*. Single dose of anti-CTLA-4 enhances CD8+ T-cell memory formation, function, and maintenance. *Proc Natl Acad Sci U S A* 2011;108:266–71.
31. Pedicord VA, Cross JR, Montalvo-Ortiz W, *et al*. Friends not foes: CTLA-4 blockade and mTOR inhibition cooperate during CD8+ T cell priming to promote memory formation and metabolic readiness. *J Immunol* 2015;194:2089–98.
32. Chen S, Lee L-F, Fisher TS, *et al*. Combination of 4-1BB agonist and PD-1 antagonist promotes antitumor effector/memory CD8 T cells in a poorly immunogenic tumor model. *Cancer Immunol Res* 2015;3:149–60.
33. Karyampudi L, Lamichhane P, Scheid AD, *et al*. Accumulation of memory precursor CD8 T cells in regressing tumors following combination therapy with vaccine and anti-PD-1 antibody. *Cancer Res* 2014;74:2974–85.

Correction: *Anti-HVEM mAb therapy improves antitumoral immunity both in vitro and in vivo, in a novel transgenic mouse model expressing human HVEM and BTLA molecules challenged with HVEM expressing tumors*

Demerlé C, Gorvel L, Mello M, *et al*. Anti-HVEM mAb therapy improves antitumoral immunity both in vitro and in vivo, in a novel transgenic mouse model expressing human HVEM and BTLA molecules challenged with HVEM expressing tumors. *J Immunother Cancer* 2023;11:e006348. doi: 10.1136/jitc-2022-006348

In the original publication, Daniel Olive was not listed as a co-corresponding author. This has now been rectified.

Check for updates

Supplemental material

BMJ Publishing Group Limited (BMJ) disclaims all liability and responsibility arising from any reliance placed on this supplemental material which has been supplied by the author(s)

J Immunother Cancer

Anti-HVEM mAb therapy improves antitumoral immunity both *in vitro* and *in vivo*, in a novel transgenic mouse model expressing human HVEM and BTLA molecules challenged with HVEM expressing tumors

Demerle C.[1,2]*, Gorvel L.[1,2]*, Mello M.[3]*, Pastor S.[2], Degos C.[1,2], Zarubica A.[3], Angelis F.[3], Fiore F.[3], Nunes J.A.[2], Malissen B.[3], Greillier L.[4], Guittard G.[2,†], Luche H.[3], Barlesi F.[5], Olive D.[1,2,†]

*these authors contributed equally to this work.

†corresponding authors

Correspondence and requests for materials should be addressed to DO or GG: daniel.olive@inserm.fr or geoffrey.guittard@inserm.fr

Supplementary methods :

Tumor Cell Lines

NCIH2291 and NICH2405 are lung adenocarcinoma cell lines purchased from ATCC and grown in RPMI supplemented with 10% FCS. HT29 is a colorectal cancer cell line grown in DMEM supplemented with 10% FCS. All cell lines were confirmed to be free of mycoplasmas using the MycoAlert detection kit (Lonza, Basel, Switzerland). Cells were detached in PBS EDTA 5mM without enzymatic solution to avoid HVEM cleavage.

Peripheral Blood Mononuclear Cells (PBMCs)

Human peripheral blood was obtained from Etablissement Francais du Sang (EFS) after obtaining informed consent from the donor. Human peripheral blood mononuclear cells (PBMC) were isolated using a Ficoll media (Eurobio) centrifuged at 800 × g for 30 min at room temperature with no break or acceleration. Cells were recovered from the interface with plasma, washed twice in PBS, counted and frozen in RPMI supplemented with 20% FCS and 10% DMSO until experimentation.

Supplemental material

BMJ Publishing Group Limited (BMJ) disclaims all liability and responsibility arising from any reliance placed on this supplemental material which has been supplied by the author(s)

J Immunother Cancer

HVEM and PD-L1 expression

Phenotypic expression was assessed by flow cytometry. HVEM expression was measured on CD4$^+$ and CD8$^+$ T cells in resting or activated conditions. 100 000 PBMC per well were distributed in 96 wells flat bottom plate, with donor specific OKT3 concentration (Ultra-LEAF Purified anti-human CD3 Antibody, Biolegend) and the following mABs when indicated: IgG1, anti-HVEM18-10, and/or anti-PD-L1 3.1 at 10 µg/ml in a final volume of 200µL RPMI supplemented with 10% FCS and 30 UI/ml IL-2 (Proleukine, Novartis). Noteworthy, OKT3 concentration was determined in advance for every PBMC donor, ranging from 5 to 50 pg/ml to obtain a sub-optimal T cells activation. Negative controls were PBMC without OKT3 and mAbs. T cell differentiation subsets were determined as: naive (CD27$^+$CD45RA$^+$), effector memory (CD27$^+$CD45RA$^-$), central memory (CD27$^-$CD45RA$^-$) and TEMRA (CD27$^-$CD45RA$^+$) (Table1). HVEM and PD-L1 expression on tumor cell lines was established twice with appropriate isotype control and viability staining.

Co-culture and proliferation assays

After thawing and overnight resting in RPMI supplemented with 10% FCS, PBMC were stained with Cell Trace Violet (CTV, Thermofisher) according to manufacturer instructions. Briefly PBMC were washed in PBS twice. CTV staining was performed at 37°c and 5% C0$_2$ for 15 minutes precisely with 1µL CTV for 10 to 15 million PBMC/ml of PBS. Then, PBMC were washed twice in RPMI supplemented with 10% FCS. PBMCs were stimulated as described above. Briefly, PBMC plated and the following mABs: IgG1, anti-HVEM18-10, and/or anti-PD-L1 3.1 and IL-2. When tumor cell lines were cultured with PBMC, they were seeded in wells 24 hours before experimentation with 50 000 cells per wells to obtain a confluence around 60%. NCIH2405 and HT29 were treated with mitomycin C at 10µg/ml (Sigma Aldrich) during 3 hours and washed three times before adding PBMC. After 72H incubation (37°c, 5% CO2) PBMC were

recovered, washed in PBS and stained at 4°c during 20 minutes with viability staining and the following antibodies: CD45, CD3, CD4, CD8, TCR-$\gamma\delta$, CD25, (Table 2). Acquisition was performed on FACS LSR II (Becton Dickinson). Application settings and sphero-beads (BD Biosciences) were used to ensure reproducible results between experiments. Data acquisition on LSRII was performed with BD DIVA software and data analysis was conducted with FlowJo (Treestar, Becton-Dickinson) software v.10.

Knock-in mouse model

To produce B6-Tnfrsf14[tm1Ciphe] KI mice in which the mouse *tnfrsf14* exon 1 was replaced with the human *tnfrsf14* exon 1, ES cells were electroporated with the vector 1477_hTNFRSF14_03_v1 (containing the human cDNA sequence TNFRSF14-001 ENST00000355716 corresponding to human TNFRSF14 exon 1). ES cells were then cultured 8 days in 96 well plate under G418 selecting conditions (250µg/mL) and screened for proper vector integration by PCRs using primers 1477_ScES_RH5_Fwd: CTCCACTGCTGCTGCTGCTCTT and 1477_ScES_RH5_Rev: GTCCCCAAACTCACCCTGAA. Southern blot analysis was used to confirm the unique integration to the correct locus. ES validated clones were then injected into Balb/cN blastocysts. Germ-line transmission, proper deletion of the Neo cassette and the presence of the sequence coding for human Tnfrsf14 was assessed by PCR (see genotyping). To produce Btla[Tm1Ciphe] mice, exon 2 from WT mouse was substituted by human exon 2.[17] The same method as described above was used to replace murine exon 2 with Btla-001 (ENSMUST00000102802) sequence. B6-Tnfrsf14[tm1Ciphe] and Btla[Tm1Ciphe] mice were then crossed to obtain double KI mice.

Genotyping

HuBTLA$^{+/+}$HuBTLA$^{+/+}$ genotyping was performed using the following PCR primers: Fwd, 5'-TGCAATGATACCTATGGTCC -3'; Rev, 5'- TGACTGTTCTGATCTGGGG -3'; with expected band sizes at 537 bp for WT alleles and 616 bp for KI. HVEM $^{hu\ KI}$ genotyping was performed using the following PCR primers: Fwd KI, 5'- CCTTACATGTTTTACTAGCCAG -3'; Fwd WT, 5'-CTGCCTCTAACAGACTTCAGT -3'; Rev, 5'- TGAAGGTGTTGTCTGTAGGG -3'; with expected band sizes at 198 bp for WT alleles and 259 for KI.

Tumor preparation for Mass cytometry and immunoprofiling

Tumors were resected from huBTLA$^{+/+}$ and DKI mice which received anti-HVEM18-10, anti-CTLA-4 or isotype treatment. Tumors were collected and digested using the Tumor Dissociation Kit (Miltenyi Biotech). Digested tumors were mechanically disrupted using the GentleMACS Octo Dissociator (Miltenyi Biotech) to obtain a single-cell suspension, followed by isolation of CD45+ TILs using the CD45 (TIL) MicroBeads kit (Miltenyi Biotech). The cells were counted before proceeding for cell surface staining. Then, tumor cells were stained for viability using Cisplatin for 10 min at 37°C, washed and stained using the panel described in supplemental table 3. Finally, cells were incubated in the presence of Iridium, a DNA intercalator allowing the identification of cells. Stained cells were then acquired on a Helios mass cytometer (Cy-TOF, Fluidigm) and analyzed using the OMIQ software platform (OMIQ).

Luminescent Label Assay :

The *CellTiter-Glo® Luminescent Cell Viability Assay* (Promega) was used to determine the number of viable cells in culture based on quantitation of the ATP present.

The intracellular amount of ATP was determined according to the manufacturer's procedures. The 96-well plate and the CellTiter-Glo® reagent was first equilibrated at room temperature for 30 min. Then an equal volume of CellTiter-Glo® Reagent is added to the volume of cell culture medium present in each well (100µL) for every tested condition. We mix contents for 2 minutes on an orbital shaker at 400 rpm to induce cell lysis. The plate is incubated at room temperature for 10 minutes to stabilize luminescent signal. Luminescence is recorded using a GloMax®-Multi+ Detection System (Program parameters: orbital shaking: 30sec, integration time: 0.1 sec, 3 reads every 5min). Data is analyzed on Prism Software.

Unsupervised CyTOF data clustering and phenotypic analysis

CyTOF data files were exported (Helios program, Fluidigm), debarcoded and live cells were gated in FlowJo (Treestar, BD). Live cell *.fcs* files were exported and analyzed using OMIQ online platform (OMIQ) (18). T cells were manually identified (TCRb$^+$CD3$^+$). T cell-gated data were subsampled to maximum equal available cell number (6000 T cells) and were subjected to an arcsinh transformation (co-factor 5). Clustering or tumor infiltrating T cells was performed using PhenoGraph (19), with the following parameters: Euclidean distance metric with K (nearest neighbor factor) =30 for cluster identification at the per mouse level. PhenoGraph clusters (n=19) were gated and displayed on a UMAP (Euclidian distance, neighbor factor 15, minimum distance 0.4) for phenotypic analysis. T cell marker expression was represented in a heatmap in function of the 19 clusters, where marker expression (columns) and clusters (rows) were subjected to hierarchical clustering using Euclidian distance (OMIQ).
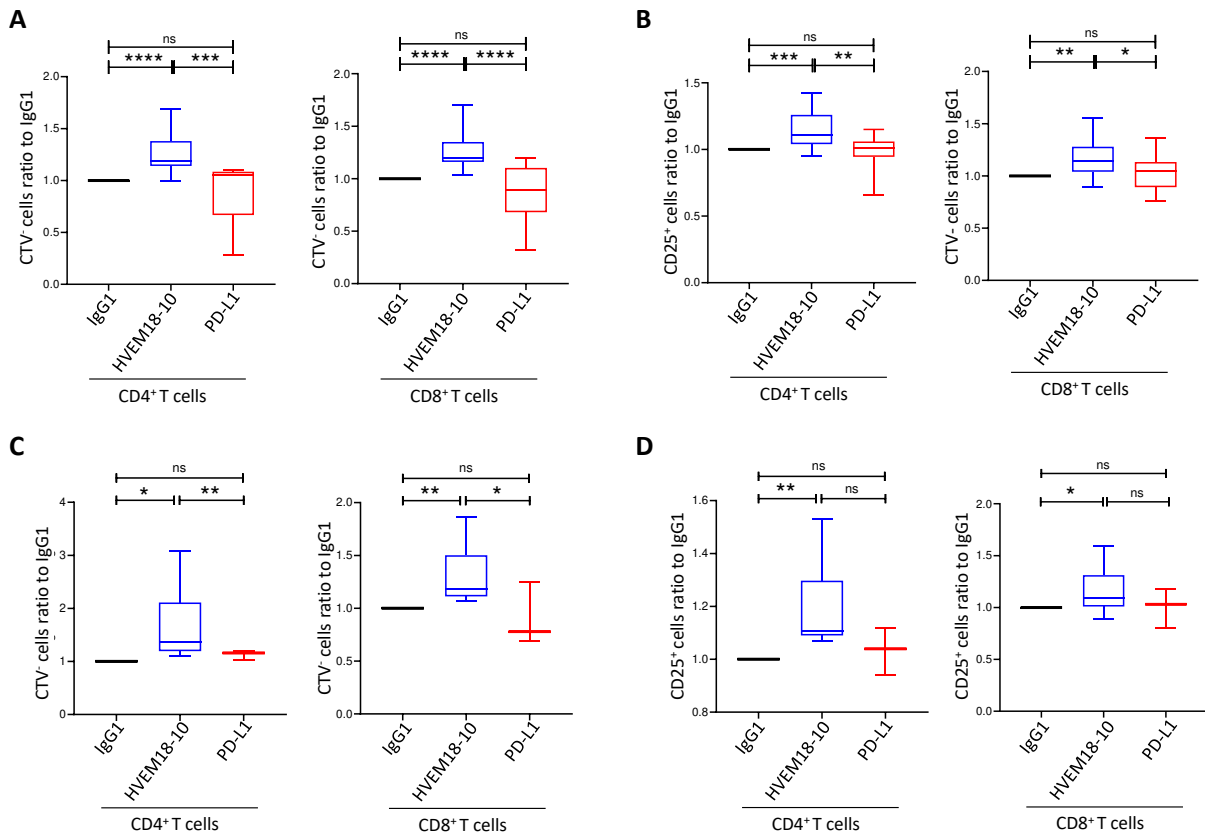
Flow cytometry for draining lymph node phenotyping.

Mice which completely rejected tumors after re-challenge had their draining lymph node (LN) resected. LNs were dissociated and stained using the panel in supplemental table 4 Stained cells were then acquired on a LSR II cytometer (Becton-Dickinson) and analyzed using the OMIQ software platform (OMIQ).
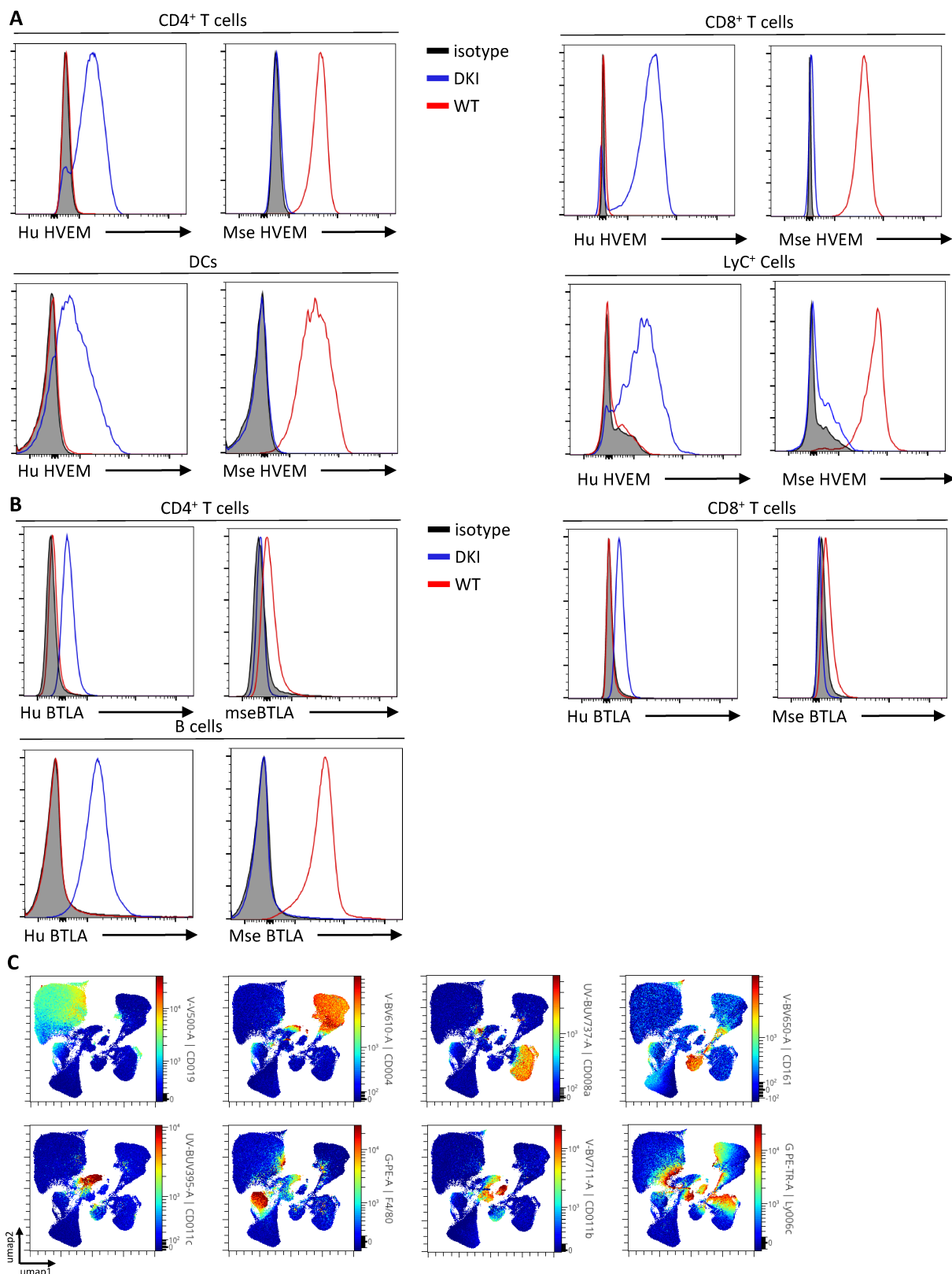
Statistical analysis

GraphPad Prism software was used to analyze and graph samples. For multiple comparison, two-way ANOVAs were performed and for comparison of condition pairs mann-whitney test was performed. *: p-val<0.05; **: p-val<0.01; ***: p-val<0.005; ****: p-val<0.001.

Supplementary figures and legends :

Supplemental material

BMJ Publishing Group Limited (BMJ) disclaims all liability and responsibility arising from any reliance placed on this supplemental material which has been supplied by the author(s)

J Immunother Cancer

Supp.Figure.1 anti-HVEM18-10 enhances T cells response against PD-L1 negative lung and colorectal cancer cell line

PD-L1 negative lung cancer NCIH2405 (A-B) or colorectal cancerHT29 (C-D) cell lines were seeded 24hours before the experiment. Then, cultured PBMC from healthy donors for 72h with OKT3 stimulation and treated or not (igG1) with anti-HVEM 18-10 antibody (blue bars/lines) or anti-PD-L1 (red bars). (A,C) proliferation profile of T cells by Cell TraceViolet staining (A for NCIH2405 and C HT29) and CD25 expression (B for NCIH2405 and D for HT29). Bar plots are the Mean ± SEM of different healthy donors samples, (A-B n=15; C-D : HVEM18-10 condition n=8 ; PD-L1 condition n =3). * $p < 0.05$, ** $p < 0.01$, *** $p < 0.005$, **** $p < 0.001$(Student's t-test)

Supplemental material

BMJ Publishing Group Limited (BMJ) disclaims all liability and responsibility arising from any reliance placed on this supplemental material which has been supplied by the author(s)

J Immunother Cancer

Supp.Figure 2 (associated to Fig5): hBTLA$^{+/+}$ and hBTLA$^{+/+}$hHVEM$^{+/+}$ Mice show similar immune cell phenotypes. A. Human or mouse HVEM expression was assessed on CD4+ , CD8+ T cells, DCs (CD11c+MHC class II+) and LyC+ cells from DKI (Blue),WT mice (red) or isotypic Ig control (black) B. Human or mouse HVEM expression on CD4+,CD8+ T and B cells cells from DKI (Blue),WT mice (red) or isotypic Ig control (black) C.Individual marker expression for the gating of each individual immune cell population.
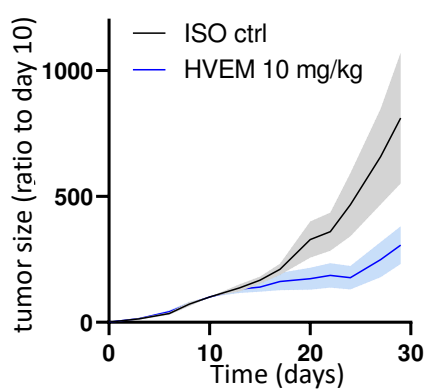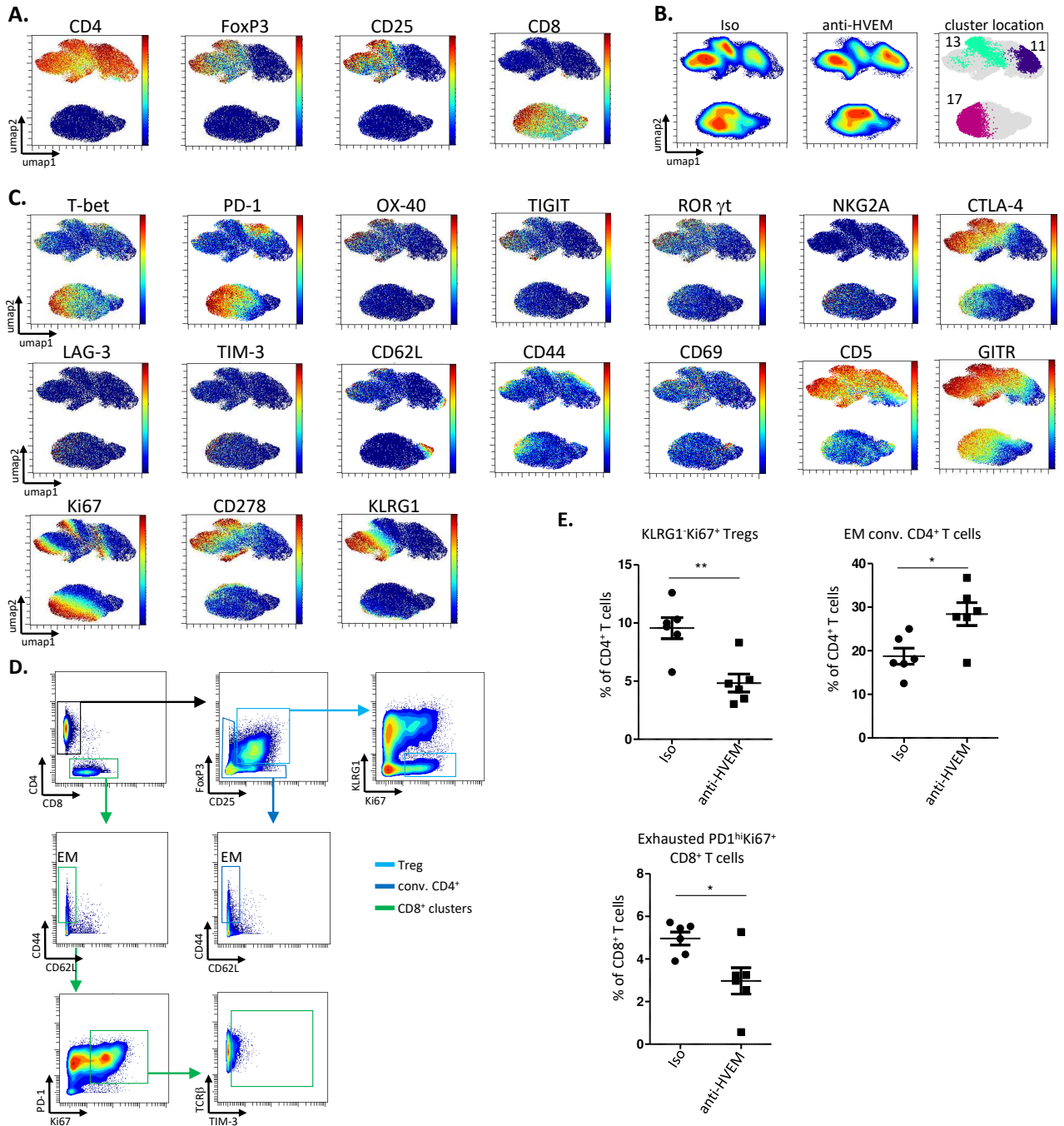
A.
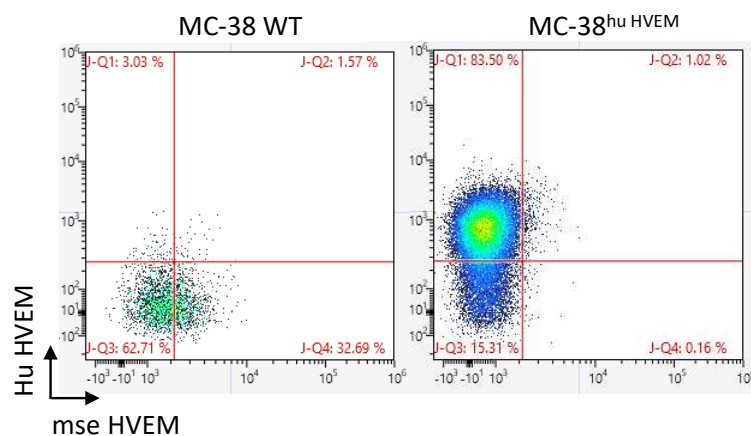
B.
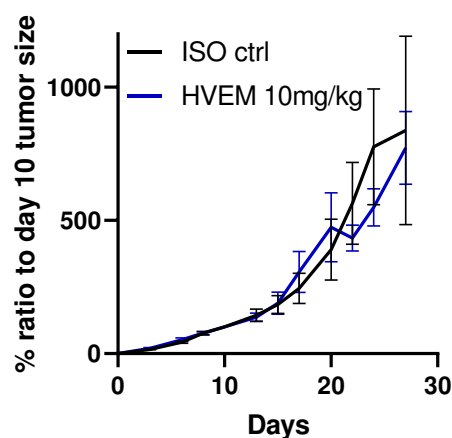
C.

Supp.Figure 3 blocking Trans-BTLA-HVEM binding *in vivo* is sufficient to decrease solid tumor growth
A.MC38-WT or MC-38 1E10 clone expression of Human or mouse HVEM in cytometry B.Measure of tumor growth showed a ratio to size of tumor at randomization day. Colorectal cancer cells MC-38$^{hu\ HVEM}$ were injected (0.5×10^6) at day 0, and Iso ct (black) or anti-HVEM 18-10 antibody 10 mg/kg (blue).

Supplemental material

BMJ Publishing Group Limited (BMJ) disclaims all liability and responsibility arising from any reliance placed on this supplemental material which has been supplied by the author(s)

J Immunother Cancer

Supp Figure 4 (associated to Fig7) : Individual marker expression, significantly modulated cluster location and manual gating validation of clusters 11, 13 and 17.
A. Main gating marker UMAP for the identification of Tregs, conventional CD4+ T cells and CD8+ T cells. **B.** Density UMAP and significantly altered cluster location. **C.** Phenotype and function marker UMAPs used to generate the heat map in Figure 8. **D.** Strategy allowing the gating of PhenoGraph clusters 11 (EM conv. CD4+ T cells), 13 (KLRG1-Ki67+ Tregs) and 17 (exhausted PD-1hiKi67+CD8+ T cells) for manual validation. **E.** Statistical validation of manually gated clusters (from D). *p.val <0.05; **p.val<0.01.
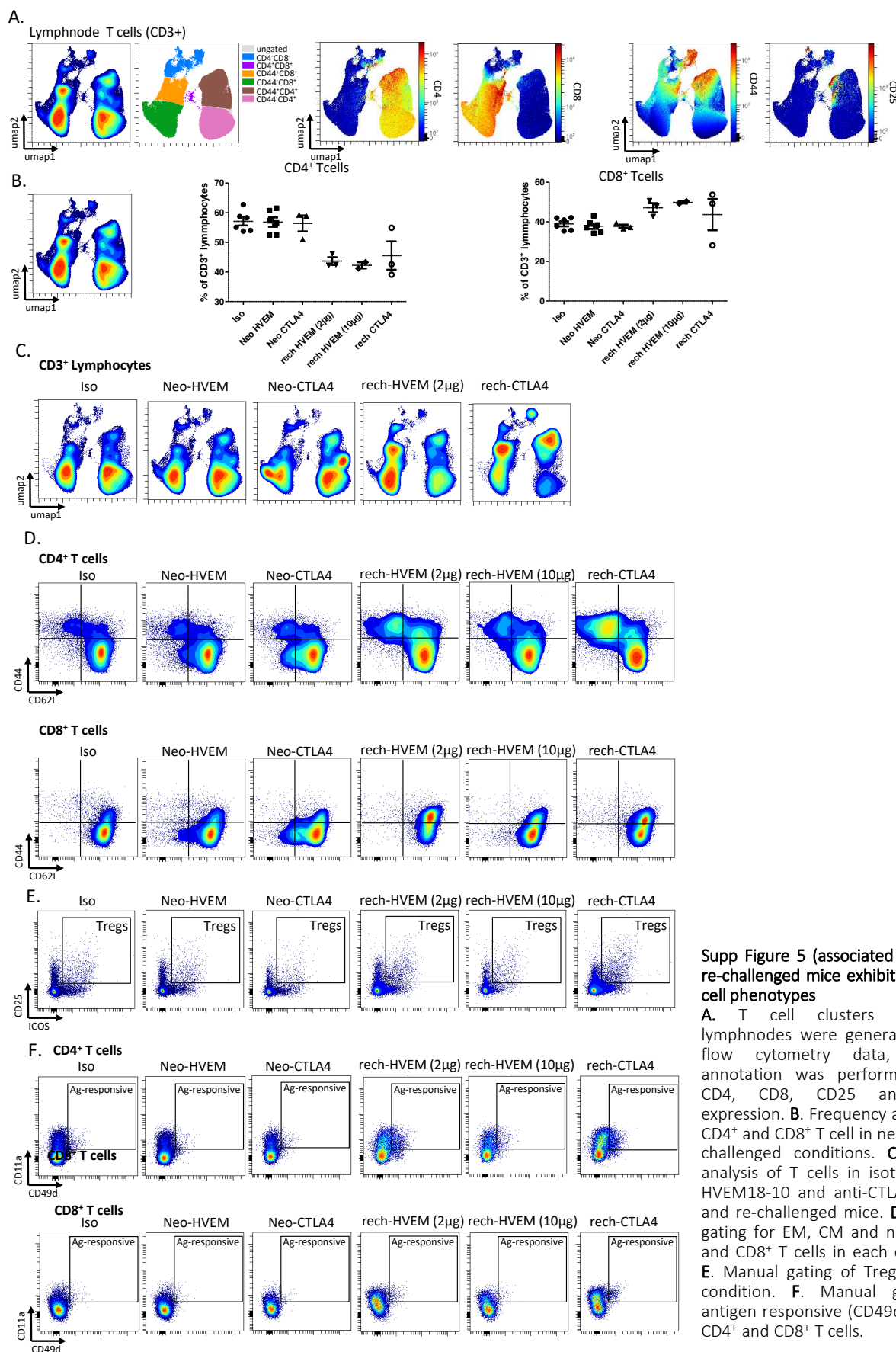
Supp Figure 5 (associated to Fig8) : re-challenged mice exhibit specific T cell phenotypes

A. T cell clusters in mice lymphnodes were generated using flow cytometry data, T cell annotation was performed using CD4, CD8, CD25 and CD44 expression. **B**. Frequency analysis of CD4+ and CD8+ T cell in neo- and re-challenged conditions. **C**. Density analysis of T cells in isotype, anti-HVEM18-10 and anti-CTLA-4 neo- and re-challenged mice. **D**. Manual gating for EM, CM and naive CD4+ and CD8+ T cells in each condition. **E**. Manual gating of Tregs in each condition. **F**. Manual gating of antigen responsive (CD49d+CD11a+) CD4+ and CD8+ T cells.